This is the peer-reviewed, final accepted version for American Mineralogist, published by the Mineralogical Society of America.
The published version is subject to change. Cite as Authors (Year) Title. American Mineralogist, in press.
DOI: https://doi.org/10.2138/am-2022-8708. http://www.minsocam.org/

Word count: ~8800 (pages 1-28) Revised Version 2

An UV/Vis/NIR optical absorption spectroscopic and color investigation of transition-metal-doped gahnite ($ZnAl_2O_4$ spinel) crystals grown by the flux method

Michail N. Taran [1], Oleksii A. Vyshnevskyi [1] and Charles A. Geiger [2,3,] *

[1] M.P. Semenenko Institute of Geochemistry, Mineralogy and Ore Formation, National Academy of Sciences of Ukraine, Palladin Ave. 34, 03680 Kyiv-142, Ukraine

[2] Department Chemistry and Physics of Materials, University of Salzburg, Jakob Haringer Str. 2a, A-5020 Salzburg, Austria

[3] Department of Mineralogy and Crystallography, University of Vienna, Josef-Holaubek-Platz 2 (UZA 2), A-1090 Vienna, Austria

* Corresponding author

Tel.: ++43-662-8044-6226

E-mail: charles.geiger@univie.ac.at

Submitted to American Mineralogist February 22, 2023

Always consult and cite the final, published document. See http:/www.minsocam.org or GeoscienceWorld

This is the peer-reviewed, final accepted version for American Mineralogist, published by the Mineralogical Society of America.
The published version is subject to change. Cite as Authors (Year) Title. American Mineralogist, in press.
DOI: https://doi.org/10.2138/am-2022-8708. http://www.minsocam.org/

Abstract

Synthetic flux-grown end-member gahnite, $ZnAl_2O_4$, and a number of different colored crystals doped with one or more transition metals including Mn Ni, Cr, Co, and Fe were studied by electron microprobe methods and UV/Vis/NIR single-crystal optical absorption spectroscopy. The first major objective was to measure and assign the various electronic absorption features. The second was to analyze quantitatively the crystal colors using the experimental spectra and the CIE 1931 color-space-chromaticity diagram. The microprobe results show that the doped gahnites have transition metal concentrations between about 0.001 and 0.1 cations per formula unit. The spectrum of colorless, nominally pure $ZnAl_2O_4$ displays no absorption in the visible region. Microprobe analysis of a light-blue gahnite crystal reveals small amounts of Ni and Mn. The UV/Vis/NIR spectrum does not indicate any dd-electronic transitions relating to Mn. All absorption features also cannot be fully interpreted using Tanabe-Sugano diagrams for Ni^{2+} in either octahedral or tetrahedral coordination. A series of seven slightly different colored gahnites with differing concentrations of Cr^{3+} and most also containing smaller amounts of Ni was investigated. The spectrum of a one pink crystal shows two intense absorption features in the visible region. They are assigned to spin-allowed $^4A_{2g} \rightarrow {}^4T_{2g}$ (^4F) and $^4A_{2g} \rightarrow {}^4T_{1g}$ (^4F) transitions of $^{VI}Cr^{3+}$. Other spectra display additional weak bands and lines that are most probably spin-forbidden dd-transitions of Ni^{2+}. These gahnites with Ni and Cr show varying purple colorations depending on the concentrations of both metals. Two more deeply blue gahnites contain Co^{2+} as demonstrated by their UV/Vis spectra but not by microprobe analysis. Two intense absorption features at ~7440 and ~16850 cm^{-1} are observed and assigned to the spin-allowed transitions $^4A_2 \rightarrow {}^4T_1$ (^4F) and $^4A_2 \rightarrow {}^4T_1$ (^4P) of Co^{2+}, respectively. Complex absorption fine structure, caused by spin-orbit and/or vibronic interactions, is also observed. Three different gahnites with yellow to orange colorations contain measurable Mn. Their spectra are similar in appearance and display a number of weak $^{IV}Mn^{2+}$ spin-forbidden transitions located above 20000 cm^{-1}. The spectra of two green gahnites show a number of Fe spin-forbidden electronic transitions arising from single, isolated $^{IV}Fe^{2+}$ and

Always consult and cite the final, published document. See http:/www.minsocam.org or GeoscienceWorld

This is the peer-reviewed, final accepted version for American Mineralogist, published by the Mineralogical Society of America.
The published version is subject to change. Cite as Authors (Year) Title. American Mineralogist, in press.
DOI: https://doi.org/10.2138/am-2022-8708. http://www.minsocam.org/

$^{VI}Fe^{3+}$ cations between 10000 and 25000 cm^{-1}. The intensities of some of the $^{VI}Fe^{3+}$-related bands can be increased through exchange-coupled interactions with next nearest $^{IV}Fe^{2+}$ neighbors. The colors of the various doped gahnites and end-member galaxite are analyzed using their single-crystal absorption spectra in the visible region. Their dominant wavelength, λ_k, and hue saturation, p_c, values are given on the CIE 1931 color-space-chromaticity diagram and are discussed. The Hex colors of all crystals are calculated and shown and they can be compared to those of the studied crystals.

Key words: Spinel, gahnite, microprobe analysis, optical absorption spectroscopy, electronic d-d transitions, crystal color, transition metal.

Always consult and cite the final, published document. See http:/www.minsocam.org or GeoscienceWorld

This is the peer-reviewed, final accepted version for American Mineralogist, published by the Mineralogical Society of America.
The published version is subject to change. Cite as Authors (Year) Title. American Mineralogist, in press.
DOI: https://doi.org/10.2138/am-2022-8708. http://www.minsocam.org/

Introduction

The oxide spinel group of phases, both natural and synthetic, consists of a large number of different end-member species. In addition, solid solution is often extensive and a great variety of compositionally intermediate crystals can be formed. Spinel can incorporate all the different metals of the first transition series, including in more than one oxidation state for some elements. For these reasons, such crystals can display a very wide range of colors. Indeed, spinels are often sold as gem stones and they are used as paint pigments. In terms of technology, $MgAl_2O_4$ crystals doped with metal ions such as Ti, Mn and Ni are used in lasers. A multitude of different types of investigations, both basic and applied in scope, have been made on the many diverse species and compositions of spinel.

Spinel is cubic with space group *Fd*-3*m* and $Z = 8$. It has the general formula $^{IV}(A_{1-x}B_x)$-$^{VI}(B_{2-x}A_x)O_4$, where A is a divalent cation and B a trivalent one. Normal and inverse spinels exist with x = 0 for the former and x = 1 for the latter. The crystal structure is based on a face-centered cubic-close-packed arrangement of oxygen anions, wherein 1/2 of them are the octahedrally and 1/8 of the tetrahedrally coordinated voids are occupied by cations. The cations lie on crystallographic special positions and are, thus, fixed by symmetry. The octahedra have shared edges that form chains parallel to [110]. The tetrahedra share corners with the octahedra. The partitioning of transition metal cations between these two coordination sites can occur in a complex manner. Ionic radii, valence states, and electronic configurations of the cations all play a role in affecting crystal-chemical properties.

Optical absorption UV/Vis/NIR spectroscopic studies have been made on both natural and synthetic spinel crystals. Different types of electronic transition behavior have been researched. Investigations on natural *sensu stricto* (*s.s.*) spinel, ideal end-member composition $MgAl_2O_4$, and gahnite, ideal end-member composition $ZnAl_2O_4$, include those of Mao et al. (1975), Dickson and Smith (1976), Taran et al. (2005, 2009), D'Ippolito et al. (2013, 2015), and Andreozzi et al. (2019). Spectra of various synthetic *s.s.* spinels have been measured by Dereń et al. (1994), Ikeda et al.

Always consult and cite the final, published document. See http:/www.minsocam.org or GeoscienceWorld

This is the peer-reviewed, final accepted version for American Mineralogist, published by the Mineralogical Society of America.
The published version is subject to change. Cite as Authors (Year) Title. American Mineralogist, in press.
DOI: https://doi.org/10.2138/am-2022-8708. http://www.minsocam.org/

(1997), Stręk et al. (1988), Hålenius et al. (2002, 2011), and Jouini et al. (2006). Synthetic gahnites have been studied by Jouini et al. (2006), Wood et al. (1968), Skogby and Hålenius (2003), Hålenius et al. (2010), and Verger et al. (2016). During the 1970s in the Soviet Union, research was undertaken to synthesize *s.s.* spinel and gahnite doped with different transition metals (e.g., Dunin-Bartkovskiy et al. 1972). The obtained flux-grown crystals show a wide range of colors. Red and blue $MgAl_2O_4$ spinels, synthesized at this time and containing chromium and cobalt, respectively, were investigated spectroscopically by Muhlmeister et al. (1993).

In this work, we study a number of synthetic gahnites, obtained from the investigation of Dunin-Bartkovskiy et al. (1972), using microprobe methods and single-crystal optical absorption UV/Vis/NIR spectroscopy. We analyze the spectra on the basis of crystal field theory and attempt to make assignments for the various absorption features. Second, the nature of the different crystal colors is studied. For this, colorimetric color calculations were made using the experimental spectra and the CIE 1931 color-space-chromaticity diagram. This is done for the first time, as best we know, using quantitative single-crystal absorption spectra.

Crystal synthesis and preparation, experimental measurements and color calculation methods

Crystal synthesis

Synthetic gahnite crystals were grown by the flux method in the1970s at the All Union Research Institute for Material Synthesis (VNIISIMS) at the Ministry of Geology of the USSR (Dunin-Bartkovskiy et al. 1972). The starting materials consisted of a stoichiometric mixture of analytical grade ZnO and Al_2O_3 powders of gahnite composition, together with MoO_3 to act as a flux. Small amounts of different transition-metal oxides, serving as "coloring agents", namely Cr_2O_3, CoO, MnO, NiO, Fe_2O_3 and CuO were added to the starting mixture. Synthesis was carried out in closed, but not sealed, alundum or porcelain crucibles having 20 to 50 cm^3 volume. The crystal synthesis was done by the method of spontaneous crystallization, whereby the charges were heated to about 1470 °C and the temperature was then decreased to 1250 °C with a cooling rate

Always consult and cite the final, published document. See http:/www.minsocam.org or GeoscienceWorld

This is the peer-reviewed, final accepted version for American Mineralogist, published by the Mineralogical Society of America.
The published version is subject to change. Cite as Authors (Year) Title. American Mineralogist, in press.
DOI: https://doi.org/10.2138/am-2022-8708. http://www.minsocam.org/

between 4.2 and 0.8 °C/h. Then, the furnace was turned off and the experiment ended. The crystal-growth period was, therefore, between 52 h and 275 h. Further details are given in the above publication.

Crystal preparation

From this broad synthesis program, sixteen variously colored and transparent gahnites (Fig. 1) were selected using a binocular microscope for microprobe analysis and UV/Vis/NIR optical absorption spectroscopic study. The crystals were prepared as platelets with thicknesses between about 0.5 to 1.0 mm (Supplementary Fig. 1). The platelets must have a proper thickness otherwise intense absorption spectroscopic features can lead to distorted bands or weak ones may go unrecorded. Care was given to assure highly polished flat and parallel surfaces in order to eliminate light scattering. This is also essential in order to obtain spectra with well-defined absorption features and well-behaved baselines.

Microprobe analysis

The chemical composition of the different gahnite samples was determined using a field-emission scanning electron microscope, JSM-6700F, equipped with an energy-dispersive spectrometer JED-2300 and a JCXA-733 electron microprobe, equipped with three wavelength-dispersive spectrometers. Both devices are located at the IGMOF NAS of Ukraine (Kyiv). For more discussion of the measuring conditions see Franz et al. (2020).

Optical absorption UV/Vis/NIR spectroscopy

Single-crystal spectra were measured in the wavelength range 330 to 1800 nm (ca. 30303-5560 cm^{-1}) using a self-constructed single-beam microspectrophotometer (see Taran et al. 2008, Taran and Vyshnevskyi 2019). The diameter of the measuring spot, fixed by the entrance and exit

Always consult and cite the final, published document. See http:/www.minsocam.org or GeoscienceWorld

This is the peer-reviewed, final accepted version for American Mineralogist, published by the Mineralogical Society of America.
The published version is subject to change. Cite as Authors (Year) Title. American Mineralogist, in press.
DOI: https://doi.org/10.2138/am-2022-8708. http://www.minsocam.org/

diaphragms of the microscope, was about 200 μm. The most transparent and homogeneously colored areas in the crystals were chosen for measurement.

Color, color simulations and calculations

A general discussion on the nature of color and the use of the CIE 1931 color-space-chromaticity diagram is given Supplementary Appendix I. It provides the background behind our color analysis of the various studied spinels.

The color investigation involved several steps. First, the measured spectra were recalculated to a standard thickness of 0.5 mm. Next, the degree of light transmission was calculated from the optical absorption coefficient in the visible range from 340 to 830 nm at wavelength intervals of $\Delta\lambda$ = 5 nm (The experimental spectra were recorded at with higher wavelength resolutions. That is, at 1 nm between 340 and 450 nm and 2 nm between 450 and 830 nm). Following this, the XYZ coordinates for each of the gahnite spectra were calculated for the C illuminator of the CIE 1931 color-space-chromaticity diagram using the "Spectral Calculator Spreadsheet" (2022). Then, the HTML color code (see https://en.wikipedia.org/wiki/Web_colors) was obtained from the XYZ coordinates using the "Easy Color Calculator" (2022). Finally, the respective Hex color for each of the studied gahnites was obtained using "ColorHexa" (2022) by entering the respective HTML color code. The resulting calculated Hex color labels are shown as insets along with the spectra given in the different figures. These calculated colors can be compared directly with those of the synthetic crystals.

Results and discussion

Gahnite crystals

The prepared gahnite platelets (Supplementary Fig. 1) were examined under an optical microscope with crossed polarizers and all crystals showed isotropic behavior. Some of the gahnites have tiny solid-phase inclusions. They occur most commonly in darker green Fe-bearing crystals

Always consult and cite the final, published document. See http:/www.minsocam.org or GeoscienceWorld

This is the peer-reviewed, final accepted version for American Mineralogist, published by the Mineralogical Society of America.
The published version is subject to change. Cite as Authors (Year) Title. American Mineralogist, in press.
DOI: https://doi.org/10.2138/am-2022-8708. http://www.minsocam.org/

and are seldom in the red to purple Cr-Ni- and blue Co-bearing gahnites. They are not observed in colorless $ZnAl_2O_4$ and in the yellow-orange Mn-bearing crystals. The inclusions are of two types. The first type is colorless and they show approximately isometric and rounded shapes, although sometimes they appear as ditrigonal plates, between about 5 and 40 microns in size. Microprobe analysis gives their chemical composition as Al_2O_3. They are considered to be corundum. The second type of inclusion is generally larger in size, typically 10 to 100 microns in size. They have MoO_3 composition, are more irregular in shape and are dark gray to black in color. Most likely they are trapped flux.

Microprobe results and gahnite compositions

The compositions of the different gahnite samples, as obtained by microprobe analysis, are given in Table 1 in terms of their calculated atoms-per-formula-unit (a.p.f.u.) values. Ghn-1 is nominally end-member $ZnAl_2O_4$ with possibly very minor Fe and Ni. The other samples, Ghn-2 to Ghn-16, contain minor or trace concentrations of one or more of Co, Ni, Cr, Mn and Fe. Cu was not detected by the methods used here. The amount of Co is always near or below the detection limit.

The crystals were checked for compositional zonation from their center to their rim. Measured profiles for Cr, Mn and Fe for samples Ghn-5, Ghn-13 and Ghn-16 are shown in Fig. 2. The Cr concentration of crystal Ghn-5 decreases from its center, having about 0.033 a.p.f.u., to the rim with about 0.020 a.p.f.u. Mn and Fe in Ghn-13 and Ghn-16, respectively, increase from roughly 0.06 a.p.f.u. at the crystal center to roughly 0.10 at the crystal rim.

UV/Vis/NIR optical absorption spectra

The different single-crystal spectra are shown in various figures and are discussed below. Table 2 lists the observed bands of the spectra, their proposed electronic assignments, where this was possible, and their wavenumbers. The calculated Hex color labels are shown in the upper right-hand corner of the figures showing the spectra

Always consult and cite the final, published document. See http:/www.minsocam.org or GeoscienceWorld

This is the peer-reviewed, final accepted version for American Mineralogist, published by the Mineralogical Society of America.
The published version is subject to change. Cite as Authors (Year) Title. American Mineralogist, in press.
DOI: https://doi.org/10.2138/am-2022-8708. http://www.minsocam.org/

211

212 **Spectrum of colorless $ZnAl_2O_4$.** Ghn-1 is end-member $ZnAl_2O_4$ or closely so. Its single-crystal
213 optical absorption spectrum is featureless in the VIS and NIR regions with the latter measured down
214 to ~5600 cm^{-1} (Fig. 3). The crystal is colorless. At the highest measured energies in the UV region,
215 weak absorption can be observed. We think it represents the low-energy edge of an intense ligand-
216 metal charge-transfer transition whose maximum occurs at higher wavenumbers. It probably arises
217 from some transition metal ion or ions, possibly Fe and/or Ni, occurring in trace concentrations.

218

219 **Spectrum of light-blue gahnite.** Light-blue gahnite Ghn-2 contains clearly measurable manganese
220 and possibly trace Co based on the microprobe results (Table 1). Its absorption spectrum shows of a
221 number of relatively weak absorption bands and lines (Fig. 3) situated on the low-energy absorption
222 edge of an oxygen-metal charge transfer transition that extends from the ultraviolet into the visible
223 region with decreasing intensity. The weak features are labeled *a* to *f* and they have peak maxima in
224 cm^{-1} at ~10000 (*a*), 15800 (*b*), 16790 (*c*), 22210 (*d*), 23420 (*e*) and 26140 (*f*). Band *b* is apparently a
225 doublet, showing a higher energy shoulder at about 15980 cm^{-1}.

226 The general appearance of these absorption features (i.e., energies, intensity ratios, widths)
227 is unlike those observed in the published spectra of different Mn^{2+}-bearing minerals and compounds
228 (e.g., Cotton et al. 1962, Goode 1965, Mehra and Venkateswarlu 1966, Huffman et al. 1969,
229 Malakhovski and Vasilev 1983, Hålenius et al. 2007, 2011). In addition, they are different from
230 those observed in the spectra of predominantly Mn^{2+}-doped gahnites that are discussed below. The
231 Mn content of Ghn-2 (Table 1) is about an order of magnitude lower than those in the Mn-bearing
232 gahnites Ghn-12, 13 and 14. Although the energy of the narrow absorption line *e* in the spectrum of
233 Ghn-2 is close to that of the line *j* in spectra of Ghn-12, 13 and 14, no other absorption feature
234 would indicate the presence of Mn^{2+}.

235 This leaves Ni as the only other transition metal to be considered in our spectroscopic
236 analysis and we consider first the possibility of Ni^{2+}. It should be noted, though, that the literature

Always consult and cite the final, published document. See http:/www.minsocam.org or GeoscienceWorld

on the optical absorption spectroscopy of Ni^{2+} in minerals is limited. Some results and interpretations obtained on synthetic crystals and compounds are, furthermore, of questionable quality and are sometimes contradictory. With this caveat in mind, we begin our analysis of the spectrum of Ghn-2. Bands *a* to *f* (Fig. 3) are unlike those observed in the spectra of various phases having Ni^{2+} in octahedral coordination (e.g., White et al. 1971, Faye 1974, Rossman et al. 1981, Manceau and Calas 1985, Manceau et al. 1985, Reddy et al. 1991, Taran et al. 2008). The sharp, relatively weak bands *b* and *e* are observed neither in the room-temperature spectra of $^{VI}Ni^{2+}$- nor $^{IV}Ni^{2+}$-bearing crystals. The spectra of ZnO, ZnS, CdS, Cs_2ZnCl and Cs_2ZnBr_4 containing some tetrahedrally coordinated Ni^{2+}, that were recorded at 78 K, do show narrow absorption lines (Weakliem 1962), but their energies are different than those of bands *b* and *e*. The spectrum of Ghn-2 is also dissimilar to that of synthetic Ni-doped $MgAl_2O_4$ spinel (Sakurai et al. 1969). The spectrum of these latter workers shows a number of absorption bands at 4500, 9300, 10150, 13200, 14000, 16000, 17000, 21000, 23200 and 27500 cm^{-1}. They were assigned to spin-allowed and spin-forbidden dd-transitions of both octahedrally and tetrahedrally coordinated Ni^{2+}. These values differ from the energies of bands *a* to *f* in the spectrum of Ghn-2. Lorenzi et al. (2006) measured the diffuse reflectance spectra of synthetic blue and green Ni-bearing gahnite powders containing small amounts of Al_2O_3 in the former and NiO in the later. The spectra of both samples show smiliar absorption features in the lower wavenumber visible region to those in the spectrum of Ghn-2 (Fig. 3). Interpretations of their powder spectra and the precise gahnite color are difficult to make because of expected band intensity differences between non-centrosymmetric tetrahedral and centosymmetric octahedral Ni^{2+} and the presence of NiO in the green smaple, respectively.

In spite of all this, we think that the absorption features in the spectrum Ghn-2 are related to Ni^{2+}. However, we cannot determine whether the Ni^{2+} is octahedrally or tetrahedrally coordinated or perhaps both. The absorption features also cannot be interpreted fully using Tanabe-Sugano (T-S) diagrams for either d^8 or d^2 electronic configurations (d^2 corresponds to Ni^{2+} in a tetrahedral crystal field - Sviridov et al. 1976, Burns 1993). We analyze the various issues. Sakurai et al. (1969)

Always consult and cite the final, published document. See http:/www.minsocam.org or GeoscienceWorld

assigned their measured bands at ~4500 and ~9300 cm^{-1} to the $^{IV}Ni^{2+}$ spin-allowed transitions $^3T_1$ (^3F) → $^3T_2$ (^3F) and $^3T_1$ (^3F) → $^3T_1$ (^3P), respectively. This agrees with an analysis using a Tanabe-Sugano diagram for the electronic d^2 configuration (Java applets 2022) with a crystal field splitting, Δ, equal to 5040 cm^{-1} and a Racah parameter *B* value of 356 cm^{-1}. If this is the case, the wavenumber of the third spin-allowed transition $^3T_1$ (^3F) → $^3A_1$ (^3F) should be about 9548 cm^{-1}, which is a little higher than that for band $^3T_1$ (^3F) → $^3T_1$ (^3P) that has a value of ~9300 cm^{-1} (Supplementary Fig. 4). This means, in contradiction to the interpretation of Sakurai et al. (1969), who assigned the band at ~17000 cm^{-1} to the latter electronic transition, no spin-allowed band of $^{IV}Ni^{2+}$ should be expected at energies greater than ~9550 cm^{-1}. It follows, therefore, that the broad and relatively intense bands *c*, *d* and *f* (Fig. 3) would be best assigned to spin-allowed transitions of $^{VI}Ni^{2+}$. We consider this possibly now.

Assume that band *a* at ~10000 cm^{-1} (Fig. 3) is, as assigned by Sakurai et al. (1969), the spin-allowed transition $^3A_{2g}$ → $^3T_{2g}$ (^3F) of $^{VI}Ni^{2+}$ (Supplementary Fig. 4). Burns (1993 - Tab. 5.19), who refers to the results of Reinen (1970)[1], gives a similar value of 9800 cm^{-1} for this band. A second spin-allowed transition of $^{VI}Ni^{2+}$, $^3A_{2g}$ → $^3T_{1g}$ (^3F), is assigned to a band at ~16000 cm^{-1} (Sakurai et al. 1969; Burns 1993) and here Δ = 9800 and *B* = 907 cm^{-1} (Burns op. cit.). We calculate for the d^8 configuration Δ = 9797 cm^{-1} and *B* = 907 cm^{-1} (Java applets 2022), which is in excellent agreement with the proposed values. Finally, the third possible spin-allowed transition of $^{VI}Ni^{2+}$, $^3A_{2g}$ → $^3T_{1g}$ (^3P) should have a wavenumber of ~27009 cm^{-1}. Burns (1993) and Sakurai et al. (1969) assigned this transition to a band at 27000 and 27500 cm^{-1}, respectively. Assuming that the first transition $^3A_{2g}$ → $^3T_{2g}$ (^3F) does have an energy of 10000 cm^{-1} (i.e., band *a* in Fig. 3), our measured intense band *c* at ~16790 cm^{-1} could be assigned to $^3A_{2g}$ → $^3T_{1g}$ (^3F). Similar calculated values are obtained using a Tanabe-Sugano diagram for an electronic d^8 configuration (Java applets 2022) taking Δ =

[1] There are differences between the reports of Reinen (1970) and Burns (1993 - Tab. 5.19). The former studied $ZnGeO_4$ spinel and the latter refers to $MgAl_2O_4$. This results in calculated values of Δ of 9500 vs. 9800 cm^{-1} and *B* of 860 vs. 907 cm^{-1}, respectively.

Always consult and cite the final, published document. See http:/www.minsocam.org or GeoscienceWorld

This is the peer-reviewed, final accepted version for American Mineralogist, published by the Mineralogical Society of America.
The published version is subject to change. Cite as Authors (Year) Title. American Mineralogist, in press.
DOI: https://doi.org/10.2138/am-2022-8708. http://www.minsocam.org/

286 10000 cm^{-1} and B = 1200 cm^{-1}. Our calculated energy of the third spin-allowed transition, $^3A_{2g} \rightarrow$
287 $^3T_{1g}$ (^3P), is then ~31222 cm^{-1}. However, the broad and intense band *f*, which is probably a spin-
288 allowed transition (Fig. 3), appears at a lower energy around 26140 cm^{-1}.

289 Summarizing our analysis, the spectrum of Ghn-2 cannot be interpreted well by Tanabe-
290 Sugano diagrams either for electronic d^8 or d^2 configurations. The narrow *b* and *e* lines should be
291 field-independent transitions (e.g., Manning 1968, Bersuker 2010). Therefore, their energy levels in
292 T-S diagrams should not change as a function of crystal field splitting as in the ground state
293 electronic levels $^3T_1$ ($^{IV}Ni^{2+}$) or $^3A_{2g}$ ($^{VI}Ni^{2+}$) - (Supplementary Figs. 4 and 5, respectively).
294 However, it appears that there are no such levels having the appropriate energies. For the Tanabe-
295 Sugano diagram of $^{IV}Ni^{2+}$ (Java applet 2022 - d^2 configuration), $^1E_1$ (^1G) has a wavenumber of
296 15713 cm^{-1} and is, therefore, similar to that of absorption line *b* with a wavenumber of 15790 cm^{-1}.
297 However, its energy should be strongly a function of crystal field splitting (Supplementary Fig. 4)
298 and, thus, a band assigned to $^3T_1$ (^3F) $\rightarrow$ ^1E (^1G) should be relatively broad.

299 It is possible that Ghn-2 could also contain some Ni^{3+} and, therefore, we consider the
300 electronic behavior of this cation as well. Once again, the literature on the optical absorption spectra
301 of Ni^{3+}-bearing phases is limited and even less so than that case for Ni^{2+}-containing phases. In an
302 early investigation, McClure (1962) measured a number of absorption bands including two features
303 at ~16500 and 19600 cm^{-1} in the spectrum of synthetic Ni^{3+}-bearing corundum. He assigned them to
304 spin-allowed crystal-field transitions of Ni^{3+}. However, there is no indication of the latter band in
305 the spectrum of Ghn-2 and the former could be masked by band *c* (Fig. 3). The diffuse reflectance
306 spectrum of Ni^{3+}-bearing $LaAlO_3$ perovskite (Sanz-Ortiz et al. 2011) shows a broad absorption
307 envelope with structure having different maxima at about 20000, 24000 and 29000 cm^{-1} and, in
308 addition, a broad band at 39300 cm^{-1}. All of them were assigned to spin-allowed electronic
309 transitions of Ni^{3+} of low-spin configuration and they are different in energy from the bands
310 observed in Ghn-2. The spectra of Ni-doped gadolinium-gallium garnet, containing both Ni^{2+} and
311 Ni^{3+} (Vasileva et al. 2012), are also different than that of Ghn-2. These workers assigned bands

Always consult and cite the final, published document. See http:/www.minsocam.org or GeoscienceWorld

This is the peer-reviewed, final accepted version for American Mineralogist, published by the Mineralogical Society of America.
The published version is subject to change. Cite as Authors (Year) Title. American Mineralogist, in press.
DOI: https://doi.org/10.2138/am-2022-8708. http://www.minsocam.org/

between ~10900 and 5200 cm^{-1} to Ni^{3+} and Ni^{2+}, whereas in the spectrum of Ghn-2 all bands occur at higher energies in the visible region except for the one located at ~10000 cm^{-1} (Fig. 3). Thus, we find no evidence for Ni^{3+} in gahnite sample Ghn-2.

To conclude, we think the observed bands labelled *a* to *f* (Fig. 3) in the spectrum of Ghn-3 are caused by Ni^{2+}. The different bands and their proposed assignments are listed in Table 2. The same is done for the other transition-metal-bearing gahnite samples discussed below.

Spectra of pink and purple gahnites. Gahnite samples Ghn-3 to Ghn-9 are all predominantly Cr-bearing and they contain some Ni as well, based on microprobe analysis. In a couple of cases, the amount of Ni is very low though, about 0.001 apfu and, here, the uncertainty might be greater than given by simple standard statistics (Indeed, the UV/Vis /IR spectra appear to provide a better determination of whether Ni is present). This may hold true for other very minor elements as well. The various microprobe-based compositions are given in Table 1.

The spectra of Ghn-3 to Ghn-8 are shown in Fig. 4. The spectra of different Cr^{3+}-bearing spinel species have been published and analyzed. We discuss these first and then we come to our gahnites. Synthetic Cr^{3+}-doped $MgAl_2O_4$ and $ZnAl_2O_4$, for example, have been studied (e.g., Hålenius et al. 2010, Verger et al. 2016). Their predominant absorption features are two broad and intense bands with maxima at about 18430 and 25870 cm^{-1}. They were assigned to the spin-allowed $^4A_{2g} \rightarrow {}^4T_{2g}$ (^4F) and $^4A_{2g} \rightarrow {}^4T_{1g}$ (^4F) electronic transitions, respectively. Another absorption feature (i.e., shoulder) was also observed at ~24200 cm^{-1}. It results from the splitting of the excited $^4T_{1g}$ (^4F) level in a slightly distorted octahedral field of point symmetry D_{3d} (Wood et al. 1968). The splitting of $^4T_{2g}$ (^4F) is much less and, therefore, it takes on a skewed band shape (Hålenius et al. 2010). In terms of our gahnites, only Ghn-6 exhibits a spectrum very similar to the published Cr^{3+}-bearing spinel spectra. That is, two intense spin-allowed bands with maxima at ~18800 and ~25650 cm^{-1} and a shoulder at ~24200 cm^{-1} are observed (Fig. 4).

Always consult and cite the final, published document. See http:/www.minsocam.org or GeoscienceWorld

This is the peer-reviewed, final accepted version for American Mineralogist, published by the Mineralogical Society of America.
The published version is subject to change. Cite as Authors (Year) Title. American Mineralogist, in press.
DOI: https://doi.org/10.2138/am-2022-8708. http://www.minsocam.org/

Spin-forbidden transitions of Cr^{3+} are not observed in the spectra of our Cr^{3+}-bearing gahnites. We do comment, though, on their occurrence in various published spectra of other spinel phases. Narrow absorption lines, termed R_1 and R_2 (i.e., a doublet), with maxima at about 14650 and 14960 cm^{-1} were observed in the spectrum of Cr^{3+}-containing $MgAl_2O_4$ recorded at 77 K (Wood et al. 1968). They were assigned to the split spin-forbidden $^4A_{2g} \rightarrow {}^2E_g$ (^2G) transition of Cr^{3+}. The spectra of synthetic $MgAl_2O_4$-$MgCr_2O_4$ and $ZnAl_2O_4$-$ZnCr_2O_4$ spinel solid solutions (Ikeda et al. 1997, Hålenius et al. 2010, Verger et al. 2016) show a relatively broad and weakly asymmetric band with a maximum at about 15000 cm^{-1} for more Cr^{3+}-rich compositions. At low Cr^{3+} contents, it is absent. The intensity of this band increases in a non-linear fashion with increasing Cr^{3+} content in the spinel. Verger et al. (2016) assigned this broad and asymmetric feature to the spin-forbidden $^4A_{2g} \rightarrow {}^2T_{1g}$ transition. We note that its energy, as given by the Tanabe-Sugano diagram for the electronic d^3 configuration (e.g., Burns 1993 - Fig. 5.24), is similar to those of the $R_{1,2}$ lines. We propose, therefore, that the differences in the intensity and broadness of the absorption feature or features at roughly 15000 cm^{-1} reflects a Cr^{3+}-Cr^{3+} exchange pairing interaction in the spinel structure. Absorption behavior is, therefore, strongly composition dependent. Why this feature is not observed, however, in the spectrum of synthetic end-member $MgCr_2O_4$ spinel (Taran et al. 2014) is not clear.

Returning to the analysis of the spectra of our other Cr^{3+}-bearing gahnites, namely Ghn-3 to Ghn-8, but not Ghn-6, we note that a number of weak absorption features with maxima at about 10000, 15800, 17000 and 28650 cm^{-1} are observed (Fig. 4 - and marked by red arrows). Ratios of band intensities are similar for all spectra, indicating that these transitions have the same physical origin. In addition, the intensities of these bands are a function of the measured Ni contents, for example, the line at ~15800 cm^{-1} (Supplementary Fig. 6). Therefore, we think that all these weak absorption features are Ni-related electronic transitions. Furthermore, the three most intense bands correspond to the *a*, *b*, and *c* bands of Ni^{2+} observed in the spectrum of Ghn-2. Note, also, that band *b* in Fig. 4 has an apparent doublet-like structure similar to that observed in Fig. 3. The higher

Always consult and cite the final, published document. See http:/www.minsocam.org or GeoscienceWorld

This is the peer-reviewed, final accepted version for American Mineralogist, published by the Mineralogical Society of America.
The published version is subject to change. Cite as Authors (Year) Title. American Mineralogist, in press.
DOI: https://doi.org/10.2138/am-2022-8708. http://www.minsocam.org/

363 wavenumber Ni^{2+} bands *d*, *e* and *f* observed in the spectrum of Ghn-2 are presumably obscured by
364 the broad intense spin-allowed band $^4A_{2g} \rightarrow {}^4T_{1g}$ (^4F) of Cr^{3+} in the spectra of samples Ghn-3 to
365 Ghn-8. The spectra of the two most Ni-rich samples, Ghn-3 and Ghn-5, also show a very weak
366 absorption feature at ~13010 cm^{-1}. It is not observed in the spectrum of Ghn-2 because the Ni
367 content is too low.
368 Because we have no information on the original intent of the gahnite synthesis experiments,
369 it is not possible to determine whether nickel oxide was added deliberately to the starting mix of a
370 number of samples in order to affect the crystal color or whether it was an unintended contaminant.
371 In terms of color, Dunin-Bartkovskiy et al. (1972) proposed that the purple color of these gahnites is
372 a result of the presence of Cr and Cu. However, the measured spectra do not show any sign of spin-
373 allowed bands of Cu^{2+} in the visible and NIR regions and no Cu was detected by microprobe
374 analysis (Table 1).
375
376 **Spectra of blue gahnites.** Gahnites Ghn-10 and Ghn-11 show more intense blue colors compared
377 to crystal Ghn-2 (Supplementary Fig. 1). The microprobe analyses of the former two samples
378 indicate very minor amounts of the transition metals Mn, Co and Ni that may possibly lie just above
379 the level of detectability (Table 1). The optical absorption spectrum of Ghn-11 is shown in Fig. 5
380 (the spectrum of Ghn-10 is similar and is not shown). It shows two broad and intense absorption
381 features centered at about 7400 and 17000 cm^{-1} and having superimposed fine structure. The
382 spectrum is similar in appearance to that of a natural Co-bearing gahnite, ignoring the Fe-related
383 bands of the latter (Taran et al. 2009). The two major bands in the spectra of the synthetic crystals
384 are also assigned to the spin-allowed $^4A_2 \rightarrow {}^4T_1$ (^4F) and $^4A_2 \rightarrow {}^4T_1$ (^4P) electronic transitions of
385 $^{IV}Co^{2+}$ of d^7 configuration, respectively. According to Bosi et al. (2012), a relatively weak spin-
386 allowed $^4A_2 \rightarrow {}^4T_2$ (^4F) band occurs at about 4000 cm^{-1} in the spectra of synthetic $(Mg_{1-x}Co_x)Al_2O_4$
387 spinels. We did not make measurements down to these lower wavenumbers.

Always consult and cite the final, published document. See http:/www.minsocam.org or GeoscienceWorld

388 The fine-structure splitting shown by the two spin-allowed bands is caused by spin-orbit
389 interactions and is often observed in the spectra of Co^{2+}-bearing phases (Taran et al. 2009 and
390 references therein).
391
392 **Spectra of yellow to orange gahnites.** Three differently yellow to orange colored gahnites, Ghn-
393 12, Ghn-13 and Ghn-14, were studied. Their compositions are given in Table 1 and Mn is the most
394 abundant transition metal. Their spectra are shown in Fig. 6 and all three are similar in appearance
395 in terms of the various absorption features. The spectra show absorption in the higher wavenumber
396 visible region that increases moving into the UV. Because manganese is the most abundant
397 transition metal in these crystals, this broad feature is interpreted as being the low-energy edge of a
398 very intense $O^{2-} \rightarrow Mn^{2+}$ charge transfer band whose maximum lies in the deeper UV region. A
399 number of absorption weaker bands and lines are superimposed on this edge. How can they be
400 assigned?
401 Consider first the spectra of a flux-grown end-member galaxite, $Mn^{2+}Al_2O_4$ (Hålenius et al.
402 2007), various composition spinels belonging to the $(Mg_{1-x}, Mn^{2+}_x)Al_2O_4$ binary (Hålenius et al.
403 2011) and a melt-grown Mn^{2+}-bearing $MgAl_2O_4$ spinel (Jouini et al. 2006). All spectra are similar
404 in appearance and they show five spin-forbidden transitions arising from tetrahedrally coordinated
405 Mn^{2+}. Hålenius et al. (2007) analyzed the spectra of a number of different Mn^{2+}-rich compounds as
406 well and they noted, once again, that five spin-forbidden bands are observed.
407 The spectra of gahnites Ghn-12, Ghn-13 and Ghn-14 display, in comparison, at least seven
408 bands some of which are narrow and weak (Fig. 6). They are labelled *g*, *h*, *i*, *j*, *k*, *l* and *m* and they
409 have maxima at about 20730, 21810, 23190, 23440, 23780, 25220 and 27190 cm^{-1}, respectively.
410 Bands *g* and *h* can be assigned to the field-dependent transitions $^4A_2$ (^6S) $\rightarrow$ $^4T_1$ (^4G) and $^4A_2$ (^6S)
411 $\rightarrow$ $^4T_2$ (^4G), as given in Table 2, and their wavenumbers indicate tetrahedral coordination of Mn^{2+}
412 (e.g., Sviridov et al. 1978). "Band" *h* shows structure and consists of at least three weakly resolved
413 components. In the spectrum of end-member galaxite (Hålenius et al. 2007) it appears as single

Always consult and cite the final, published document. See http:/www.minsocam.org or GeoscienceWorld

Gausian-like absorption band, labelled ν_2 and having a wavenumber of 22250 cm^{-1}. "Band" *i* also shows some structure, that is a doublet with two maxima at ~23120 and ~23230 cm^{-1}. Both "band" *i* and band *j* have wavenumbers typical for the field-independent $^6A_1 \rightarrow {}^4A_1$, ^4E (^4G) transitions of tetrahedrally coordinated Mn^{2+}, where "band" *i* corresponds to $^6A_1 \rightarrow {}^4E$ and *j* to $^6A_1 \rightarrow {}^4A_1$. In the spectra of galaxite (Hålenius et al. 2007) and Mn^{2+}-bearing *s.s.* spinels (Jouini et al. 2006, Hålenius et al. 2011), $^6A_1 \rightarrow {}^4A_1$, ^4E (^4G) is characterized by just a single band at about 23400 cm^{-1}. The precise nature of this electronic transition in the various spinel species may be related to the symmetry of the local $Mn^{2+}O_4$ tetrahedra in their respective crystal structures. Our Mn^{2+}-poor gahnites may possibly have $Mn^{2+}O_4$ groups somewhat distorted from T_d symmetry causing $^6A_1 \rightarrow {}^4A_1$ and $^6A_1 \rightarrow {}^4E$ to have slightly different energies.

The nature of band *k* is not fully clear. An assignment to the $^6A_1 \rightarrow {}^2T_2$ (^2I) transition is unlikely because it should be weaker because $\Delta S = 2$, than spin-forbidden transitions with $\Delta S = 1$ given, for example, by the bands *g*, *h*, *i*, *j* and *l*. To the best of our knowledge, this transition of energy 23780 cm^{-1} has not been observed in the spectra of any Mn^{2+}- or Fe^{3+}-bearing compounds[2]. The narrow band *l* at ~25200 cm^{-1} can be assigned to the transition $^6A_1 \rightarrow {}^4T_2$ (^4D). Its energy is lower than that of a band at 25970 cm^{-1} observed in the spectrum of galaxite (Hålenius et al. 2007). Band *m* at ~27190 cm^{-1} in the spectra of Ghn-12 and Ghn-13 (Fig. 6) occurs as a weak feature superimposed on the intense high-energy ligand-metal absorption edge. It is assigned (Table 2) to the field-independent transition $^6A_1 \rightarrow {}^4E$ (^4D). It is observed at about 27780 cm^{-1} in the spectra of end-member galaxite (Hålenius et al. 2007) and Mn^{2+}-doped $MgAl_2O_4$ spinels (Jouini et al. 2006).

Bosi et al. (2007) assigned two broad absorption bands at 21200 and 10800 cm^{-1}, occurring on an intense high-energy edge in the spectra of Mn-rich $MgAl_2O_4$-$MgMn_2O_4$ solid solutions, to spin-allowed crystal-field transitions of octahedral and tetrahedral Mn^{3+}, respectively. Because there is no indication of an absorption band at about 10800 cm^{-1} in the spectra of gahnites Ghn12 - Ghn14 (Fig. 6), we assume that only a small amount of manganese in the crystals could occur as $^{VI}Mn^{3+}$. It

[2] Fe^{3+} and Mn^{2+} have a d^5 electronic configuration.

Always consult and cite the final, published document. See http:/www.minsocam.org or GeoscienceWorld

439 could substitute for Zn at the tetrahedral site and contribute to the intense UV absorption edge at
440 about 21000 cm^{-1}.

441 We note that in all three of our gahnites, Ghn-12, Ghn-13, Ghn-14, there are small but
442 measurable amounts of Fe (Table 1). It may occur as Fe^{3+} and, thus, cause increased absorption in
443 the UV region due to the presence of an intense $O^{-2} \rightarrow Fe^{3+}$ ligand-metal charge-transfer band. This
444 may also explain why the spectrum of synthetic end-member iron-free galaxite (Hålenius et al.
445 2007) shows very weak absorption between 20000 and 25000 cm^{-1}, although its Mn content is one
446 order of magnitude greater than that in Ghn-12, Ghn-13 and Ghn-14.
447
448 **Analysis of crystal field and Racah parameters.** Electrostatic repulsion occurs among electrons in
449 an atom. For an ion in the free state (i.e., $\Delta = 0$ or $Dq = 0$), the total interelectronic repulsion can be
450 described by the so-called Racah parameters *A*, *B* and *C*. For crystals, *B* and *C* can be calculated
451 from the measured energies of the field-independent Mn^{2+} spin-forbidden electronic transitions $^6A_1$
452 $\rightarrow$ $^4A_1$, ^4E (^4G) and $^6A_1 \rightarrow$ ^4E (^4D), as described by Moore and White (1972) and Hålenius et al.
453 (2007). We analyze and discuss the value of these parameters in Appendix II (supplementary
454 information).
455
456 **Spectra of green gahnites**. Gahnites Ghn-15 and Ghn-16 have Fe as the most abundant transition
457 metal (Table 1). The spectra of both are shown in Fig. 7. They differ in appearance from the spectra
458 of flux-grown $MgAl_2O_4$-$Fe^{2+}Al_2O_4$ solid solutions (Hålenius et al. 2002), but are similar to the
459 spectra of natural type II *s.s.* spinel-hercynite and gahnite-hercynite solid solutions (Taran et al.
460 2005). Spectra of the latter system showed various spin-forbidden bands that were assigned to
461 single, "isolated" $^{IV}Fe^{2+}$ and $^{VI}Fe^{3+}$ ions, and also bands reflecting local Fe^{2+}-Fe^{3+} pairs indicating
462 electronic exchange coupling. The coupling occurs between iron cations located in adjacent
463 octahedral and tetrahedral coordination sites.

Always consult and cite the final, published document. See http:/www.minsocam.org or GeoscienceWorld

This is the peer-reviewed, final accepted version for American Mineralogist, published by the Mineralogical Society of America.
The published version is subject to change. Cite as Authors (Year) Title. American Mineralogist, in press.
DOI: https://doi.org/10.2138/am-2022-8708. http://www.minsocam.org/

464 The spectra of Ghn-15 and Ghn-16 indicate different electronic transition types. At the
465 highest wavenumbers, the low-energy edge of a very intense ligand-metal charge-transfer
466 absorption feature, possibly $O^{2-} \rightarrow Fe^{2+}$ and/or $O^{2-} \rightarrow Fe^{3+}$, is observed. In the NIR region
467 absorption related to the high-energy flank of a spin-allowed $^5E \rightarrow {}^5T_2$ band of $^{IV}Fe^{2+}$ (Taran et al.
468 2005) occurs. Between these two intense absorption features, a number of weaker bands can be
469 observed. A number of them are labeled as *r*, *q*, *p*, *o* and *n* (note that band *o* is not observable, but
470 can be obtained through curve-fitting the spectra of natural spinels) and they are assigned to various
471 spin-forbidden transitions of Fe^{3+}. The narrow band *q* is typical for a field-independent transition
472 and it can be assigned to $^6A_{1g} \rightarrow {}^4A_{1g}$, ^4E_g (^4G) of $^{VI}Fe^{3+}$ (Taran et al. 2005). The sharp peak at
473 about 22000 cm^{-1} is diagnostic of Fe^{3+} in minerals (Burns 1993). The intensity of band *q* could be
474 enhanced by "borrowing" some intensity from an $O^{2-} \rightarrow Fe^{3+}$ charge-transfer transition in the case
475 their energies overlap. Its intensity could also be increased through electronic exchange involving
476 coupled Fe^{3+}-Fe^{2+} pairs, as could those of the other Fe^{3+} bands as well (Taran et al. 2005, Andreozzi
477 et al. 2019). A second field-independent transition, $^6A_{1g} \rightarrow {}^4E_g$ (^4D) of Fe^{3+}, at higher energy could
478 be expected from the Tanabe-Sugano diagram for the electronic $3d^5$ configuration, but it is probably
479 obscured by the very intense $O^{2-} \rightarrow Fe^{3+}$ charge-transfer edge. In the spectra of Fe^{3+}-bearing
480 minerals a narrow band appears between 26000 and 27000 cm^{-1} (Burns 1993) and is frequently
481 more intense than the band $^6A_{1g} \rightarrow {}^4A_{1g}$, ^4E_g (^4G). Band *r* (Fig. 7) is likely the $^6A_{1g} \rightarrow {}^4T_{2g}$ (^4D)
482 transition of $^{VI}Fe^{3+}$, which is typically much less intense than the two above noted field-independent
483 bands $^6A_{1g} \rightarrow {}^4A_{1g}$, ^4E_g (^4G) and $^6A_{1g} \rightarrow {}^4E_g$ (^4D). The relatively broad bands *n* and *p* may be spin-
484 forbidden $^6A_{1g} \rightarrow {}^4T_{2g}$ and $^6A_{1g} \rightarrow {}^4T_{1g}$ transitions of $^{VI}Fe^{3+}$, whose intensities are affected, once
485 again, by a $^{VI}Fe^{3+}$-$^{IV}Fe^{2+}$ pair interaction (Taran et al. 2005). Band *o* may be a split component of
486 the $^6A_{1g} \rightarrow {}^4T_{1g}$ transition of $^{VI}Fe^{3+}$, caused by trigonal distortion of the octahedral site in the spinel
487 structure (point symmetry $\bar{3}m$) (Taran et al. 2005).
488 Because other transition metals occur in very low concentrations (0.002 a.p.f.u. or less)
489 based on the microprobe results, the weak absorption features at ~17260, 18030 and 19600 cm^{-1} are

Always consult and cite the final, published document. See http:/www.minsocam.org or GeoscienceWorld

also probably related to Fe (Fig. 7 and shown by red arrows). They may possibly be spin-forbidden bands of single, "isolated" $^{IV}Fe^{2+}$ cations, although, as noted by Taran et al. (2005), who observed similar absorption features in the spectra of a natural spinel of type II, their intensity does not correlate well with iron content. They could not exclude that they could be caused by the presence of $^{IV}Co^{2+}$. As discussed above, the spin-allowed bands of $^{IV}Co^{2+}$ are intense, see (Fig. 5), even at very minor concentrations of cobalt.

Colorimetric analysis

In terms of spinel, as best we know, color calculations have only been made on synthetic $Zn(Al_{2-x},Cr^{3+}_x)O_4$ crystals obtained on powder diffuse reflectance spectra (Verger et al. 2016). We consider, here, the color of our gahnites using their single-crystal optical absorption spectra in the visible region together with the CIE 1931 color-space-chromaticity diagram. This allows a quantitative description and analysis of the different crystal colors.

Figure 8 shows the loci of the colors for the different transition-metal-doped gahnites of this work as well as that of end-member galaxite (Hålenius et al. 2007) all normalized to a sample thickness of 0.5 mm. A photo of twelve gahnite platelets of approximately 1 mm thickness (Supplementary Fig. 1), which was made under day-light illumination, allows a comparison of calculated and observed colors. To describe chromaticity with the CIE diagram, the dominant wavelength, λ_k, and the hue saturation value, p_c, are better suited than the parameters *x* and *y*. λ_k (or the complementary λ_k') give the dominant spectral hue (or purple colors that are mixtures of red and blue). The hue saturation parameter, p_c, gives the amount of spectral color (or various purple colorations) that is mixed with white light (point C) needed to reproduce a given color having the coordinates x and y. It can vary between 0 and 1 in value. What can be concluded in terms of the colors of the different gahnite crystals investigated here?

Both the Ni-doped (Ghn-2) and Co-doped (Ghn-10 and Ghn-11) gahnites have a predominant blue coloration. The former sample has a weak greenish tint with λ_k = 498.5 nm

Always consult and cite the final, published document. See http:/www.minsocam.org or GeoscienceWorld

compared to the two latter crystals that are distinctly deeper blue with $\lambda_k \approx 480.5$ nm. Its low p_c value of 0.01 indicates that the color is pale. The colors of Ghn-10 and Ghn-11 show higher saturation and their p_c values are 0.20 and 0.22, respectively. Therefore, they plot farther from the locus C than Ghn-2 (Fig. 8). Although Ni-bearing and Co-bearing gahnites are both blue, their spectra are very different. In the case of Ghn-10 and 11, the spin-allowed $^4A_2 \rightarrow {}^4T_1$ (^4P) Co^{2+} transition gives rise to a broad band that absorbs the green, yellow, orange and red components (Fig. 5) of the white illuminating light. Blue, and to a lesser extent violet radiation - whereby the latter is less sensitive to the human eye than the former - are transmitted. The spectrum of Ghn-2 is very different. The spin-forbidden absorption bands of Ni^{2+} (Fig. 3) are much weaker compared to the spin-allowed Co^{2+} band in the visible region. Transmittance is greatest in the blue region and, partly but less so, in the green and yellow regions. A weak greenish blue coloration result.

The loci of the six studied Cr^{3+}-(Ni^{2+})-bearing gahnites are located below C in the purple region (Fig. 8). Their crystal colors are largely determined by the two intense spin-allowed transitions of Cr^{3+} with their absorption centered in the violet and green regions. The pink-red color of Ghn-6, whose sole transition metal is Cr^{3+} as based on spectroscopy, is the simplest to interpret. The spectra of the other gahnites of this series show the presence of Ni^{2+} and they affect the crystal colorations. These gahnites are shown from right (Ghn-6) to left (Ghn-5) in Fig. 8. Their color variations reflect the degree of transmission of red light due to the presence of the two Ni^{2+} absorption bands *c* and *b*. The λ_k' values vary from ~499 nm for Ghn-6 to ~561 nm for Ghn-5. The values of color saturation, p_c, are rather low, varying from 0.08 for Ghn-7 to 0.17 for Ghn-5.

The three Mn^{2+}-bearing gahnites, Ghn-12, 13, and 14, have spectra that are complex, showing a number of absorption features. The $O^{2-} \rightarrow Mn^{2+}$ charge transfer edge and the different spin forbidden bands lead to absorption above 19000 cm^{-1} in the higher energy part of the visible region. The calculated colors of the three samples are yellow-orange with varying tints and saturations. The values of λ_k and p_c are 574.5 nm and 0.28 (Ghn-12), 575 nm and 0.33 (Ghn-13), and 576 nm and 0.49 (Ghn-14). The color of end-member galaxite was calculated using the

Always consult and cite the final, published document. See http:/www.minsocam.org or GeoscienceWorld

This is the peer-reviewed, final accepted version for American Mineralogist, published by the Mineralogical Society of America.
The published version is subject to change. Cite as Authors (Year) Title. American Mineralogist, in press.
DOI: https://doi.org/10.2138/am-2022-8708. http://www.minsocam.org/

spectrum of Hålenius et al. (2007), which was digitalized, and it is shown for comparison. It has a λ_k value of ~573 nm, which is the closest to the green region of the four Mn^{2+}-containing spinels. Its p_c value of ~0.58 is the largest of all the samples and reflects its high Mn^{2+} content.

The spectra of Fe-bearing gahnites Ghn-15 and Ghn-16 show varying absorption over the entire visible region. This arises from the low-energy oxygen → Fe charge transfer edge and the different spin-forbidden Fe bands of various energies. The colors of the two crystals mainly arise from the relatively low absorption in the two windows of light transmission occurring in the green and blue regions centered at about 22500 and 20000 cm^{-1}, respectively (see Andreozzi et al. 2019, their Fig. 10). The loci of Ghn-15 and Ghn-16 have the same λ_k value of ~564 nm, but they differ in their p_c values of ~0.06 and ~0.23, respectively.

In closing, we note that the two-dimensional CIE color diagram cannot fully describe the true colors and nuances of coloration of different gahnite crystals because color should be represented three dimensionally. The third important coordinate is brightness y' (see "Color and color simulations and calculations" – see Appendix I) and it is not considered in this analysis. The use of Hex color labels overcomes, at least partly, this limitation.

For those interested in a detailed discussion of optical colorimetry, we recommend the excellent treatment of Judd and Wyszecki (1963).

Implications

Owing to their various chemical and thermal stabilities, mechanical hardness, as well as interesting electrical and thermomechanical properties, different composition spinels have or could have a number of technological applications. They are also of importance as gems and for use as pigments in paints. Crystal engineering is an ongoing research field and the spinel group provides a vast compositional system for further investigation.

The results of this study show the need for more UV/Vis/NIR spectroscopic measurements in order to understand more fully detailed crystal-chemical behavior that cannot, for example, be provided by diffraction measurements. The nature and origin of crystal color was investigated and it

Always consult and cite the final, published document. See http:/www.minsocam.org or GeoscienceWorld

This is the peer-reviewed, final accepted version for American Mineralogist, published by the Mineralogical Society of America.
The published version is subject to change. Cite as Authors (Year) Title. American Mineralogist, in press.
DOI: https://doi.org/10.2138/am-2022-8708. http://www.minsocam.org/

568 was discussed how this can be done in a quantitative manner. Little work has been done on this
569 subject in the field of mineralogy. Other minerals and/or mineral groups, both natural and synthetic,
570 need investigation in this direction. Research needs to be done to make crystal color descriptions
571 more quantitative and to understand better the chemical and physical origins of color. Finally, we
572 note that more advanced model calculations than provided by simple crystal field theory and
573 Tanabe-Sugano diagrams are needed to interpret optical absorption spectra more completely and
574 correctly.
575

576 **Acknowledgments**

577 We thank Ulf Hålenius for helpful discussion concerning the spectra of Mn-bearing spinels. He also
578 gave a constructive review that improved the paper as did a second anonymous referee.
579

Always consult and cite the final, published document. See http:/www.minsocam.org or GeoscienceWorld

This is the peer-reviewed, final accepted version for American Mineralogist, published by the Mineralogical Society of America.
The published version is subject to change. Cite as Authors (Year) Title. American Mineralogist, in press.
DOI: https://doi.org/10.2138/am-2022-8708. http://www.minsocam.org/

References

Andreozzi, G.B., D'Ippolito, V., Skogby, H., Hålenius, U., and Bosi, F. (2019) Color mechanisms in spinel: a multi-analytical investigation of natural crystals with a wide range of coloration. Physics and Chemistry of Minerals, 46, 343-360.

Bersuker, I.B. (2010) Electronic Structure and Properties of Transition Metal Compounds: Introduction to the Theory. 2nd ed., John Wiley and Sons. 759 p.

Bosi, F., Hålenius, U., D'Ippolito, V., and Andreozzi, G.B. (2012) Blue spinel crystals in the $MgAl_2O_4$-$CoAl_2O_4$ series: Part II. Cation ordering over short-range and long-range scales. American Mineralogist, 97, 1834-1840.

Burns, R.G. (1993) Mineralogical Applications of Crystal Field Theory. Cambridge University Press, Cambridge, England. 551 p.

ColorHexa (2022) - https://www.colorhexa.com/669999.

Cotton, F.A., Goodgame, D.M.L., and Goodgame, M. (1962) Absorption spectra and electronic structure of some tetrahedral manganese (II) complexes. Journal of the American Chemical Society, 84, 167-172.

D'Ippolito, V., Andreozzi, G.B., Bosi, F., Hålenius, U., Mantovani, L., Bersani, D., and Fregola, R. A. (2013) Crystallographic and spectroscopic characterization of a natural Zn-rich spinel approaching the endmember gahnite ($ZnAl_2O_4$) composition. Mineralogical Magazine, 77, 2941-2953.

D'Ippolito, V., Andreozzi, G.B., Hålenius, U., Skogby, H., Hametne, K., and Günther, D. (2015) Color mechanisms in spinel: cobalt and iron interplay for the blue color. Physics and Chemistry of Minerals, 42, 431-439.

Dereń, P.J., Stręk, W., Oetliker, U., Güdel, H.U. (1994) Spectroscopic properties of Co^{2+} ions in $MgAl_2O_4$ spinels. Physica Status Solidi (b), 182, 241-251.

Always consult and cite the final, published document. See http:/www.minsocam.org or GeoscienceWorld

This is the peer-reviewed, final accepted version for American Mineralogist, published by the Mineralogical Society of America.
The published version is subject to change. Cite as Authors (Year) Title. American Mineralogist, in press.
DOI: https://doi.org/10.2138/am-2022-8708. http://www.minsocam.org/

605 Dickson, B.L., and Smith, G. (1976) Low temperature optical absorption and Mössbauer spectra of
606 staurolite and spinel. Canadian Mineralogist, 14, 206-215.
607 Dunin-Bartkovskiy, R.L., Klientova. G.P., and Lisitsina, E.E. (1972) Getting spinels from the
608 solutions in a melt of molybdenum anhydrite. In: The experimental investigations of mineral
609 formation in dry oxide and silicate systems (Lakin, V.V. ed.). Moscow, Nauka, 1972, 255-257
610 (in Russian).
611 Easy Color Calculator (2022) - http://www.easyrgb.com/en/create.php.
612 Ercan, F., Ates, T., Kaygili, O., Bulut, N., Koytepe, S., Alahmari, F., Ercan, I., and Hssain, A.H.
613 (2021) Investigation of the effects of Ni-doping on the structural and thermal properties of
614 $ZnAl_2O_4$ spinels prepared by wet chemical method. Journal of the Australian Ceramic
615 Society, 57, 1155-1162.
616 Faye, G.H. (1974) Optical absorption spectrum of Ni^{2+} in garnierite, a discussion. Canadian
617 Mineralogist, 12, 389–393.
618 Franz G., Vyshnevskyi, O., Taran, M., Khomenko, V., Wiedenbeck, M., Schiperski, F., and Nissen,
619 J. (2020) A new emerald occurrence from Kruta Balka, Western Peri-Azovian region,
620 Ukraine: Implications for understanding the crystal chemistry of emerald. American
621 Mineralogist, 105, 162-181.
622 Goode, D.H. (1965) Optical absorption spectrum of Mn^{2+} in cubic and tetragonal ligand fields.
623 Journal of Chemical Physics, 43, 2830-2840.
624 Hålenius, U., Andreozzi, G.B., and Skogby, H. (2010) Structural relaxation around Cr^{3+} and the
625 red-green color change in the spinel (sensu stricto)-magnesiochromite ($MgAl_2O_4$-$MgCr_2O_4$)
626 and gahnite-zincochromite ($ZnAl_2O_4$-$ZnCr_2O_4$) solid-solution series. American Mineralogist,
627 95, 456-462.
628 Hålenius, U., Bosi, F., and Skogby, H. (2007) Galaxite, $MnAl_2O_4$, a spectroscopic standard for
629 tetrahedrally coordinated Mn^{2+} in oxygen-based mineral structures. American Mineralogist,
630 92, 1225-1231.

Always consult and cite the final, published document. See http:/www.minsocam.org or GeoscienceWorld

This is the peer-reviewed, final accepted version for American Mineralogist, published by the Mineralogical Society of America.
The published version is subject to change. Cite as Authors (Year) Title. American Mineralogist, in press.
DOI: https://doi.org/10.2138/am-2022-8708. http://www.minsocam.org/

631 Hålenius, U., Bosi, F., and Skogby, H. (2011) A first record of strong structural relaxation of TO_4
632 tetrahedra in a spinel solid solution. American Mineralogist, 96, 617-622.
633 Hålenius, U., Skogby, H., and Andreozzi, G.B. (2002) Influence of cation distribution on the optical
634 absorption spectra of Fe^{3+}-bearing spinel s.s.-hercynite crystals: evidence for electron
635 transitions in $^{VI}Fe^{2+}$-$^{VI}Fe^{3+}$ clusters. Physics and Chemistry of Minerals, 29, 319-330.
636 Huffman, D.R., Wild, R.L., and Shinmei, M. (1969) Optical absorption spectra of crystal-field
637 transitions in MnO. Journal of Chemical Physics, 50, 4092-4094.
638 Ikeda, K., Nakamura, Y., Masumoto, K., and Shima, H. (1997) Optical spectra of synthetic spinels
639 in the system $MgAl_2O_4$-$MgCr_2O_4$. Journal of the American Chemical Society, 80, 2672-2676.
640 Java applets (2022) - http://wwwchem.uwimona.edu.jm/courses/Tanabe-Sugano/TSapplets.html.
641 Jouini, A., Sato, H., Yoshikawa, A., Fukuda, T., Boulon, G., Kato. K., and Hanamura, E. (2006)
642 Crystal growth and optical absorption of pure and Ti, Mn-doped $MgAl_2O_4$ spinel. Journal of
643 Crystal Growth, 287, 313-317.
644 Judd, D.B. and Wyszecki, G. (1963) Color in Business, Science, and Industry. New York, John
645 Wiley and Sons, Inc., 500 pp.
646 Lorenzi, G., Baldi, G., Di Benedetto, F., Faso V., Lattanzi, P. and Romanelli, M. (2006)
647 Spectroscopic study of a Ni-bearing gahnite pigment. Journal of the European Ceramic
648 Society, 26, 317-321.
649 Malakhovski, A.V. and Vasilev, G.G. (1983) Covalence as source of intensity for d-d transitions in
650 octahedral complexes. Physica Status Solidi (b), 118, 337-344.
651 Manceau A., Calas, G., and Decarreau, A. (1985) Nickel-bearing clay minerals: I. Optical
652 spectroscopic study of nickel crystal chemistry. Clay Minerals, 20, 367-387.
653 Manceau, A. and Calas, G. (1985) Heterogeneous distribution of nickel in hydrous silicates from
654 New Caledonia ore deposits. American Mineralogist, 70, 549-558.
655 Manning, P.G. (1968) Absorption spectra of the manganese-bearing chain silicates pyroxmangite,
656 rhodonite, bustamite and serandite. Canadian Mineralogist, 9, 348-357.

Always consult and cite the final, published document. See http:/www.minsocam.org or GeoscienceWorld

This is the peer-reviewed, final accepted version for American Mineralogist, published by the Mineralogical Society of America.
The published version is subject to change. Cite as Authors (Year) Title. American Mineralogist, in press.
DOI: https://doi.org/10.2138/am-2022-8708. http://www.minsocam.org/

657 Mao, H.K. and Bell, P.M. (1975) Crystal-field effects in spinel: oxidation states of iron and
658 chromium. Geochimica et Cosmochimica Acta, 39, 869-871.
659 McClure, D.S. (1962) Optical spectra of transition metal ions in corundum. Journal of Chemical
660 Physics, 36, 2757-2779.
661 Mehra, A. and Venkateswarlu, P. (1966) Absorption spectrum of Mn^{2+} in KCI. Journal of Chemical
662 Physics, 45, 3381-3383.
663 Muhlmeister, S., Koivula, J.I., Kammerling, R.C., Smith C.P., Fritsch, E., and Shigley, J.E. (1993)
664 Flux-grown synthetic red and blue spinels from Russia. Gems and Gemology, 26, 81-98.
665 Reddy, B.C.V., Kumar D.S.S., and Kumar R.R. (1991) Optical absorption spectrum of Ni^{2+} ions in
666 ammonium dihydrogen phosphate. Physica Scripta, 44, 263-264.
667 Reinen, D. (1970) Kationenverteilung zweiwertiger $3d^n$-Ionen in oxidischen Spinell-, Granat- und
668 anderen Strukturen. Structure and Bonding, 7, 114-154.
669 Rossman, G.R., Shannon, D., and Waring, R.C. (1981) Origin of the yellow color of complex nickel
670 oxides. Journal of Solid State Chemistry, 39, 277-287.
671 Sakurai, T., Ishigame, M., and Arashi, H. (1969) Absorption spectrum of Ni^{2+} ions in spinel.
672 Journal of Chemical Physics, 50, 3241-3245.
673 Sanz-Ortiz, M.N., Rodríguez, F., Rodríguez, J., and Demazeau, G. (2011) Optical and magnetic
674 characterization of Co^{3+} and Ni^{3+} in $LaAlO_3$: interplay between the spin state and Jahn-Teller
675 effect. Journal of Physics: Condensed Matter, 23, 415501 (6pp).
676 Skogby, H. and Hålenius, U. (2003) An FTIR study of tetrahedrally coordinated ferrous iron in the
677 spinel-hercynite solid solution. American Mineralogist, 88, 489-492.
678 Spectral Calculator Spreadsheet (2022) - http://www.brucelindbloom.com/.
679 Stręk, W., Dereń, P.J., and Jezowska-Trżebiatowska B. (1988) Optical properties of Cr^{3+} in
680 $MgAl_2O_4$ spinel. Physica B: Condensed Matter, 152, 379-384.

Always consult and cite the final, published document. See http:/www.minsocam.org or GeoscienceWorld

This is the peer-reviewed, final accepted version for American Mineralogist, published by the Mineralogical Society of America.
The published version is subject to change. Cite as Authors (Year) Title. American Mineralogist, in press.
DOI: https://doi.org/10.2138/am-2022-8708. http://www.minsocam.org/

Sviridov, D.T., Sviridova, R.K., Kulik, N.I., and Glasko, V.B. (1978) Investigation of the optical spectra of crystals containing Mn^{2+} ions. Zhurnal Prikladnoi Spektroskopii, 29, 924-926 (in Russian).

Sviridov, D.T., Sviridova, R.K., and Smirnov, Yu.F. (1976) Optical spectra of transition metal ions in crystals. Moscow, Nauka, 266 p. (in Russian).

Taran, M.N., Koch-Müller, M., and Feenstra, A. (2009) Optical spectroscopic study of tetrahedrally coordinated Co^{2+} in natural spinel and staurolite at different temperatures and pressures. American Mineralogist, 94, 1647-1652.

Taran, M.N., Koch-Müller, M., and Langer, K. (2005) Electronic absorption spectroscopy of natural (Fe^{2+}, Fe^{3+})-bearing spinels of spinel s.s.-hercynite and gahnite-hercynite solid solutions at different temperatures and high-pressures. Physics and Chemistry of Minerals, 32, 175-188.

Taran, M.N., Ohashi, H., and Koch-Müller, M. (2008) Optical spectroscopic study of synthetic $NaScSi_2O_6$–$CaNiSi_2O_6$ pyroxenes at normal and high pressures. Physics and Chemistry of Minerals, 35, 117-127.

Taran, M.N., Parisi, F., Lenaz, D., and Vishnevskyy, A.A. (2014) Synthetic and natural chromium bearing spinels: an optical spectroscopy study. Physics and Chemistry of Minerals, 41, 593-602.

Taran, M.N. and Vyshnevskyi, O.A. (2019) Be, Fe^{2+}-substitution in natural beryl: an optical absorption spectroscopy study. Physics and Chemistry of Minerals, 46, 795-806.

Vasileva, N.V., Gerus, P.A., Sokolov, V.O. and Plotnichenko, V.G. (2012) Optical absorption of Ni^{2+} and Ni^{3+} ions in gadolinium gallium garnet epitaxial films. Journal of Physics D: Applied Physics, 45, 485301 (8 pp).

Verger, L., Dargaud, O., Rousse, G., Rozsályi, E., Juhin, A., Cabaret, D., Cotte, M., Glatzel, P., and Cormier, L. (2016) Spectroscopic properties of Cr^{3+} in the spinel solid solution $Zn(Al_{1-x}Cr_x)_2O_4$. Physics and Chemistry of Minerals, 43, 33-42.

Always consult and cite the final, published document. See http:/www.minsocam.org or GeoscienceWorld

This is the peer-reviewed, final accepted version for American Mineralogist, published by the Mineralogical Society of America.
The published version is subject to change. Cite as Authors (Year) Title. American Mineralogist, in press.
DOI: https://doi.org/10.2138/am-2022-8708. http://www.minsocam.org/

706 Weakliem, H.A. (1962) Optical spectra of Ni^{2+}, Co^{2+}, and Cu^{2+} in tetrahedral sites in crystals.
707 Journal of Chemical Physics, 36, 2117-2139.
708 White W.B. and Mccarthy G.J., and Scheetz B.E. (1971) Optical spectra of chromium, nickel, and
709 cobalt-containing pyroxenes. American Mineralogist, 56, 72-89.
710 Wood, D.L., Imbusch, G.F., Macfarlane, R.M., Kisliuk, P., and Larkin, D.M. (1968) Optical
711 spectrum of Cr^{3+} ions in spinels. Journal of Chemical Physics, 48, 5255-5263.

Always consult and cite the final, published document. See http:/www.minsocam.org or GeoscienceWorld

This is the peer-reviewed, final accepted version for American Mineralogist, published by the Mineralogical Society of America.
The published version is subject to change. Cite as Authors (Year) Title. American Mineralogist, in press.
DOI: https://doi.org/10.2138/am-2022-8708. http://www.minsocam.org/

712 Table 1. Gahnite sample labels, their platelet thicknesses used for spectroscopic measurement and their compositions.

Sample	Thickness (mm)	n	a.p.f.u. (atoms per formuala unit) calculated on the basis of four O atoms*								
			Al	Cr	Fe	Mn	Co	Ni	Cu	Zn	Total
Ghn-1	0.48	6	2.000 (0.004)	b.d.	0.001 (0.0004)	b.d.	b.d.	0.001 (0.0005)	b.d.	0.998 (0.002)	3.000
Ghn-2	0.68	5	2.000 (0.003)	b.d.	b.d.	0.008 (0.002)	0.001 (0.0005)	0.005 (0.001)	b.d.	0.985 (0.003)	2.999
Ghn-3	0.72	7	1.987 (0.003)	0.013 (0.001)	0.001 (0.0005)	0.001 (0.0002)	0.001 (0.0002)	0.009 (0.001)	b.d.	0.989 (0.002)	3.001
Ghn-4	1.02	5	1.978 (0.008)	0.022 (0.002)	0.001 (0.0004)	0.001 (0.0005)	0.002 (0.0009)	0.008 (0.002)	b.d.	0.987 (0.006)	2.999
Ghn-5(c)	0.83	7	1.962 (0.005)	0.038 (0.004)	0.002 (0.0007)	0.001 (0.0005)	b.d.	0.024 (0.002)	b.d.	0.972 (0.008)	2.999
Ghn-6	0.62	6	1.966 (0.007)	0.034 (0.004)	0.001 (0.0005)	b.d.	b.d.	0.001 (0.0005)	b.d.	0.996 (0.003)	2.998
Ghn-7	1.05	5	1.983 (0.007)	0.017 (0.002)	b.d.	0.001 (0.0004)	0.001 (0.0005)	0.006 (0.001)	b.d.	0.992 (0.008)	3.000
Ghn-8	0.67	5	1.983 (0.007)	0.017 (0.002)	0.004 (0.001)	0.003 (0.001)	b.d.	0.001 (0.0005)	b.d.	0.991 (0.005)	2.999
Ghn-9	0.68	7	1.982 (0.009)	0.018 (0.001)	0.002 (0.0008)	0.002 (0.001)	0.001 (0.0005)	0.002 (0.0008)	b.d.	0.991 (0.007)	2.998
Ghn-10	0.91	5	2.000	b.d.	b.d.	0.001	0.001	0.001	b.d.	0.995	2.998

Always consult and cite the final, published document. See http:/www.minsocam.org or GeoscienceWorld

This is the peer-reviewed, final accepted version for American Mineralogist, published by the Mineralogical Society of America.
The published version is subject to change. Cite as Authors (Year) Title. American Mineralogist, in press.
DOI: https://doi.org/10.2138/am-2022-8708. http://www.minsocam.org/

			(0.004)			(0.0004)	(0.0004)	(0.0003)		(0.004)	
Ghn-11	1.09	6	2.000 (0.003)	b.d.	b.d.	0.001 (0.0004)	0.002 (0.0008)	0.002 (0.0006)	b.d.	0.995 (0.003)	3.000
Ghn-12	0.68	6	1.999 (0.004)	0.001 (0.0004)	0.004 (0.001)	0.082 (0.005)	0.001 (0.0002)	0.001 (0.0004)	b.d.	0.912 (0.012)	3.000
Ghn-13(c-r)	0.60	7	1.999 (0.004)	0.001 (0.0005)	0.003 (0.001)	0.077 (0.002)	b.d.	0.001 (0.0005)	b.d.	0.920 (0.007)	3.001
Ghn-14	0.82	6	2.000 (0.004)	b.d.	0.003 (0.001)	0.095 (0.003)	b.d.	0.003 (0.001)	b.d.	0.899 (0.008)	3.000
Ghn-15	1.05	6	1.999 (0.004)	0.001 (0.0004)	0.054 (0.002)	0.001 (0.0004)	b.d.	b.d.	b.d.	0.944 (0.006)	2.999
Ghn-16(c-r)	0.81	7	1.999 (0.004)	0.001 (0.0005)	0.085 (0.003)	0.001 (0.0005)	b.d.	0.002 (0.0008)	b.d.	0.912 (0.010)	3.000

(c) – core; (c-r) – intermediate between core and rim; n – number of point analyses;

*- the average value over n;

b.d. – below the detection limit (0.0007-0.0009 a.p.f.u. for Cr, Fe, Mn, Co, Ni, Cu); values in parentheses are the standard deviation.

Always consult and cite the final, published document. See http:/www.minsocam.org or GeoscienceWorld

This is the peer-reviewed, final accepted version for American Mineralogist, published by the Mineralogical Society of America.
The published version is subject to change. Cite as Authors (Year) Title. American Mineralogist, in press.
DOI: https://doi.org/10.2138/am-2022-8708. http://www.minsocam.org/

Table 2. Energies of the absorption bands measured in the optical spectra of the various transition-metal-doped synthetic gahnites and their electronic dd-transition assignments (see text).

Samples & Spectra	Chromophore	Absorption band (cm^{-1})	Electronic transition
Ghn-2 - Fig. 3	Ni^{2+}	a: 10000	$^{IV}Ni^{2+}$: $^3A_{2g} \rightarrow {}^3T_{2g}$ (^3F)
		b: 15800	n. a.
		c: 16790	$^{IV}Ni^{2+}$: $^3A_{2g} \rightarrow {}^3T_{1g}$ (^3F)
		d: 22210	n. a.
		e: 23420	n. a.
		f: 26140	n. a.
Ghn-3 - Ghn-9 - Fig. 4	Cr^{3+} and Ni^{2+}	a: 10000	$^{IV}Ni^{2+}$: $^3A_{2g} \rightarrow {}^3T_{2g}$ (^3F)
		b: 15800	Ni^{2+}: n. a.
		c: 17000	$^{IV}Ni^{2+}$: $^3A_{2g} \rightarrow {}^3T_{1g}$ (^3F)
		18470	Cr^{3+}: $^4A_{2g} \rightarrow {}^4T_{2g}$ (^4F)
		24000, 25900	Cr^{3+}: $^4A_{2g} \rightarrow {}^4T_{1g}$ (^4F)
		28280	Ni^{2+}: n. a.
Ghn-10 - Ghn-11 - Fig. 5	Co^{2+}	6670, 7030, 7770, 7990, 8150	$^4A_2 \rightarrow {}^4T_1$ (^4F)
		16110, 16850, 17260, 18240	$^4A_2 \rightarrow {}^4T_1$ (^4P)
		20960	$^4A_2$ (^4F) $\rightarrow {}^2T_1$ (^2G)
Ghn-12 - Ghn-14 - Fig. 6	Mn^{2+}	g: 20730	$^4A_2$ (^6S) $\rightarrow {}^4T_1$ (^4G)
		h: 21680, 21810, 22240	$^4A_2$ (^6S) $\rightarrow {}^4T_2$ (^4G)
		i: 23100 – 23240	$^6A_1 \rightarrow {}^4E$
		j: 23440	$^6A_1 \rightarrow {}^4A_1$
		k: 23780	n. a.
		l: 25200	$^6A_1 \rightarrow {}^4T_2$ (^4D)
		m: 27190	$^6A_1 \rightarrow {}^4E$ (^4D)
Ghn-15 - Ghn-16 - Fig. 7	Fe^{3+} and Fe^{2+}	n: 10900	$^{VI}Fe^{3+}$: $^6A_{1g} \rightarrow {}^4T_{2g}$ (^4G)
		o: 13020, p: 15040	$^{VI}Fe^{3+}$: $^6A_{1g} \rightarrow {}^4T_{1g}$ (^4G)
		17350	$^{IV}Fe^{2+}$: n. a.
		18040	$^{IV}Fe^{2+}$: n. a.
		19610	$^{IV}Fe^{2+}$: n. a.
		q: 21690	$^{VI}Fe^{3+}$: $^6A_{1g} \rightarrow {}^4A_{1g}$, ^4E_g ^4G)
		r: 23190	$^{VI}Fe^{3+}$: $^6A_{1g} \rightarrow {}^4T_{2g}$ (^4D)

n.a. - not assigned

Always consult and cite the final, published document. See http:/www.minsocam.org or GeoscienceWorld

This is the peer-reviewed, final accepted version for American Mineralogist, published by the Mineralogical Society of America.
The published version is subject to change. Cite as Authors (Year) Title. American Mineralogist, in press.
DOI: https://doi.org/10.2138/am-2022-8708. http://www.minsocam.org/

Figures

Fig. 1. Synthetic gahnites grown by the flux method. The size of the crystals varies from about 1.5 to 5 mm. Different types of habits and/or morphologies can be distinguished (all not necessarily shown here). The first one, which is relatively rare, displays euhedral crystals with flat smooth faces and sharp edges. The second, also rare, shows flattened (111) twins. A third rather unusual type, shows octahedra having square pits at the vertices. The fourth, most common crystal type, includes individuals with several triangular growth plates of variable thickness on {111} octahedral faces. This gives rise to a stepped-like appearance. Aggregates of different crystal types can also be observed.

Fig. 2. Cr, Mn and Fe concentration profiles measured from the center to the rim of crystals Ghn-5, Ghn-13 and Ghn-16, respectively. The intensity of the red Cr-doped gahnites Ghn-3 to Ghn-9 is the same through the crystals. The intensity of the orange Mn-doped gahnites Ghn-12 to Ghn-14 and the green Fe-bearing gahnites Ghn-15 and Ghn-16 increases distinctly near the rims of the crystals.

Fig. 3. Optical absorption spectra of end-member $ZnAl_2O_4$, Ghn-3 (below), and nickel-doped gahnite, Ghn-2 (above). The spin-forbidden bands of Ni^{2+} are labelled *a* to *f* and are shown by the arrows. Calculated color labels are shown (in the following figures as well) and were obtained as discussed in the text.

Fig. 4. Optical absorption spectra of chromium-doped gahnites Ghn-3 to Ghn-8. The spectra are shifted vertically from one another for the sake of clarity. The three spin-allowed bands of $^{VI}Cr^{3+}$ are marked by the black arrows. The bands of Ni^{2+} (see Fig. 3 for comparison) are marked by red arrows and labeled as for Ghn-2.

Fig. 5. Optical absorption spectrum of cobalt-doped gahnite Ghn-11.

Always consult and cite the final, published document. See http:/www.minsocam.org or GeoscienceWorld

This is the peer-reviewed, final accepted version for American Mineralogist, published by the Mineralogical Society of America.
The published version is subject to change. Cite as Authors (Year) Title. American Mineralogist, in press.
DOI: https://doi.org/10.2138/am-2022-8708. http://www.minsocam.org/

754

755 Fig. 6. Optical absorption spectra of manganese-doped gahnites Ghn-12, Ghn-13 and Ghn-14. The
756 color of synthetic galaxite, $Mn^{2+}Al_2O_4$, with a thickness of 0.5 mm was calculated by digitalizing
757 the spectrum in Hålenius et al. (2007). They state that the color of their galaxite with a thickness of
758 0.103 mm is yellow.

759

760 Fig. 7. Optical absorption spectra of iron-doped gahnites Ghn-15 and Ghn-16. The bands *f*, *m*, *n*, *p*
761 and *q*, as marked by black arrows, are assigned to spin-forbidden transitions of Fe^{3+}. They can be
762 intensified through electronic exchange with neighboring Fe^{2+} cations (i.e., local Fe^{3+}-Fe^{2+} pairs).
763 The weak absorption features, indicated by red arrows and not labeled by letters, may be spin-
764 forbidden bands of "isolated" single $^{IV}Fe^{2+}$ cations.

765

766 Fig. 8. CIE 1931 color-space-chromaticity diagram (see Appendix I) showing the loci of the various
767 transition-metal-doped gahnites (Ghn 2 to 16) and that of end-member galaxite (G) calculated from
768 the spectrum of Hålenius et al. (2007) that was first digitalized. C is the locus of the standard
769 illuminator and represents scattered Northern daylight.

770

771

772

773

774

775

776

777

778

779

780

Always consult and cite the final, published document. See http:/www.minsocam.org or GeoscienceWorld

This is the peer-reviewed, final accepted version for American Mineralogist, published by the Mineralogical Society of America.
The published version is subject to change. Cite as Authors (Year) Title. American Mineralogist, in press.
DOI: https://doi.org/10.2138/am-2022-8708. http://www.minsocam.org/

822
823
824
825
826 Fig. 1.
827

Always consult and cite the final, published document. See http:/www.minsocam.org or GeoscienceWorld

This is the peer-reviewed, final accepted version for American Mineralogist, published by the Mineralogical Society of America.
The published version is subject to change. Cite as Authors (Year) Title. American Mineralogist, in press.
DOI: https://doi.org/10.2138/am-2022-8708. http://www.minsocam.org/

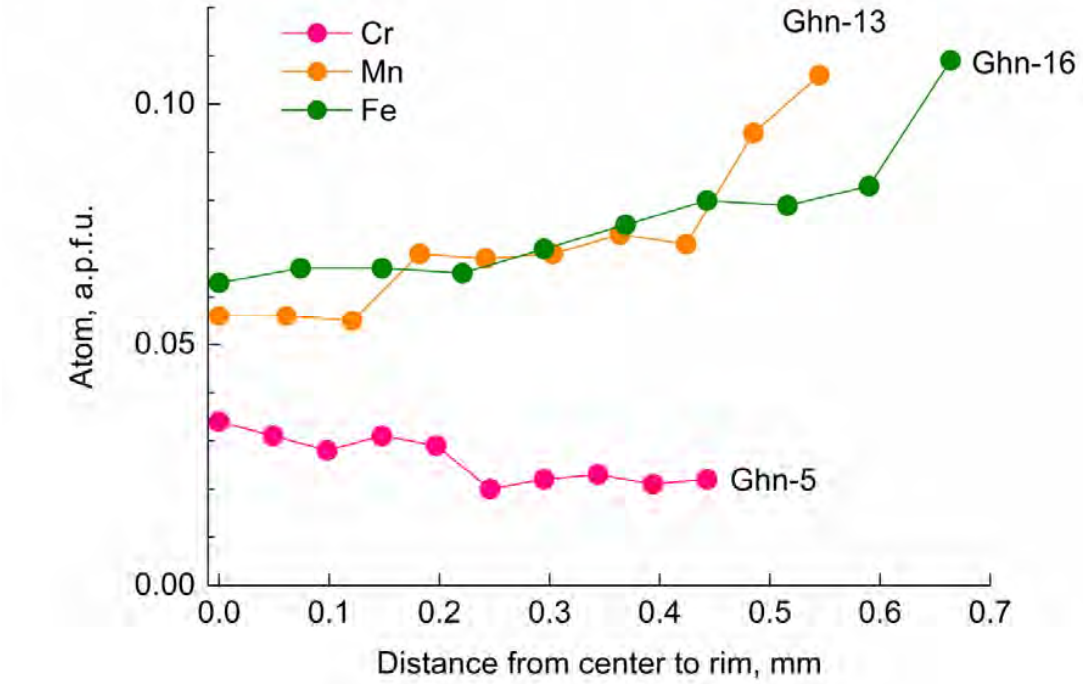

828

829

830

831 Fig. 2.

832

833

Always consult and cite the final, published document. See http:/www.minsocam.org or GeoscienceWorld

This is the peer-reviewed, final accepted version for American Mineralogist, published by the Mineralogical Society of America.
The published version is subject to change. Cite as Authors (Year) Title. American Mineralogist, in press.
DOI: https://doi.org/10.2138/am-2022-8708. http://www.minsocam.org/

834

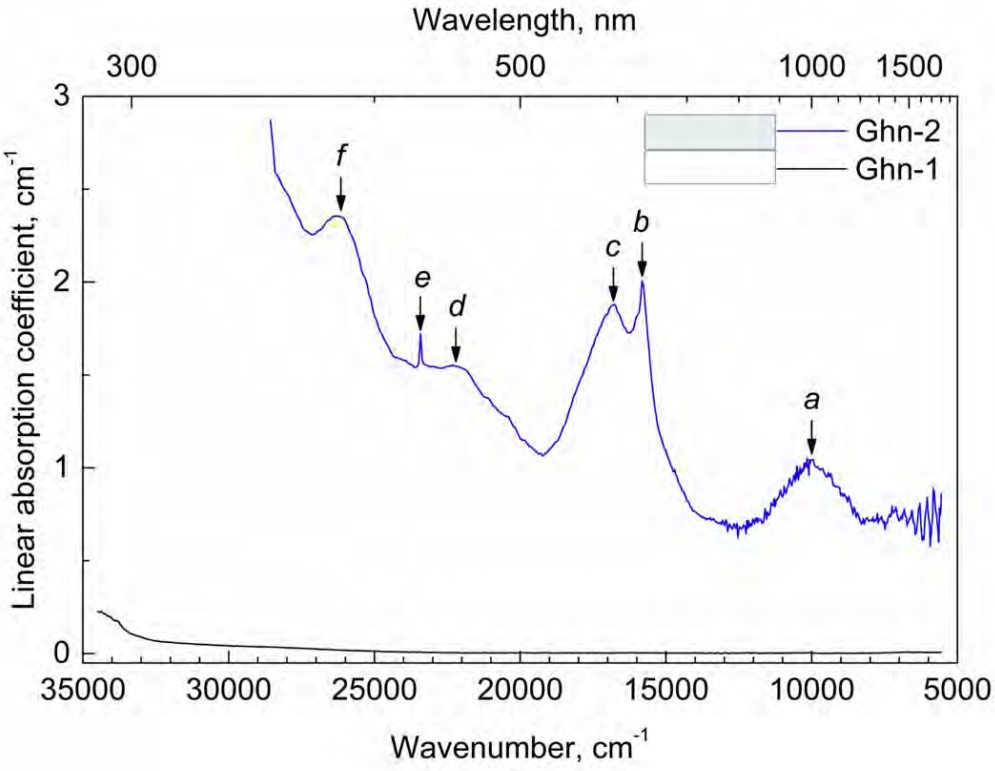

8

836

837

838

839 Fig. 3.

Always consult and cite the final, published document. See http:/www.minsocam.org or GeoscienceWorld

This is the peer-reviewed, final accepted version for American Mineralogist, published by the Mineralogical Society of America.
The published version is subject to change. Cite as Authors (Year) Title. American Mineralogist, in press.
DOI: https://doi.org/10.2138/am-2022-8708. http://www.minsocam.org/

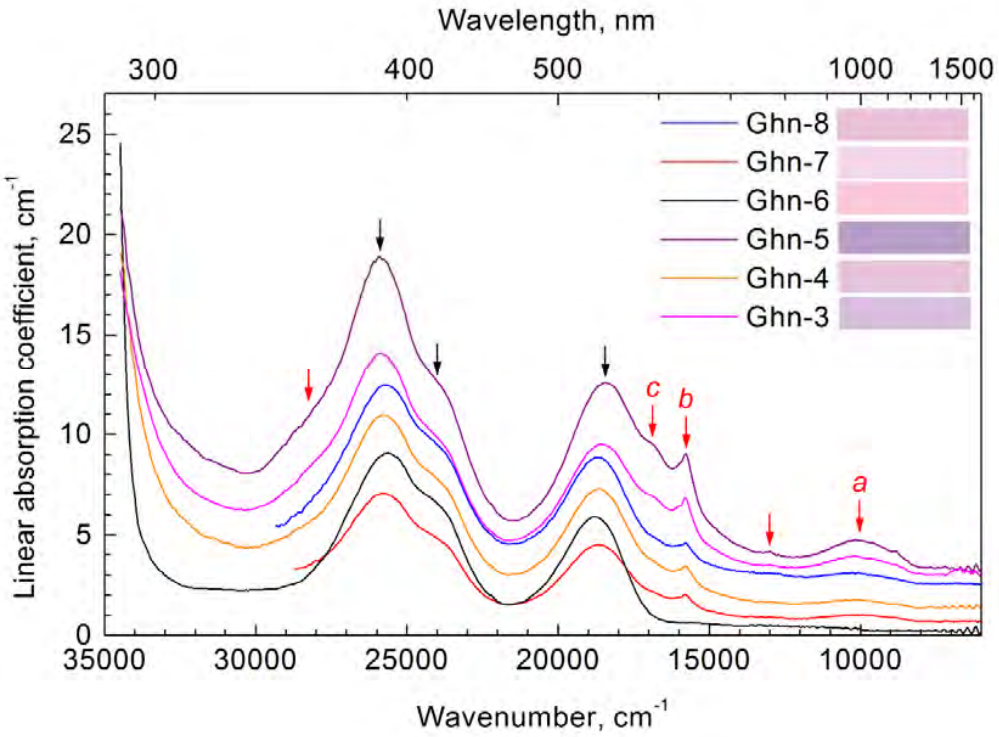

840

841

842

843

844 Fig. 4.

845

Always consult and cite the final, published document. See http:/www.minsocam.org or GeoscienceWorld

This is the peer-reviewed, final accepted version for American Mineralogist, published by the Mineralogical Society of America.
The published version is subject to change. Cite as Authors (Year) Title. American Mineralogist, in press.
DOI: https://doi.org/10.2138/am-2022-8708. http://www.minsocam.org/

846

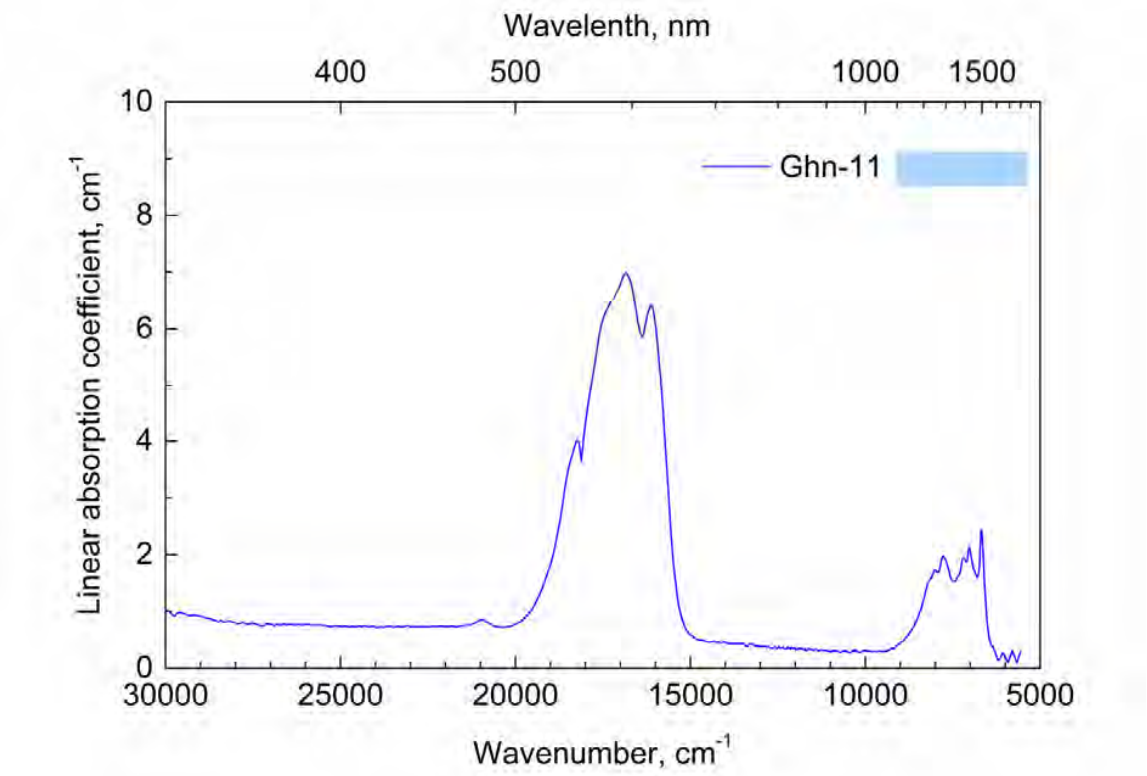

847

848

849

850

851 Fig. 5.

852

Always consult and cite the final, published document. See http:/www.minsocam.org or GeoscienceWorld

This is the peer-reviewed, final accepted version for American Mineralogist, published by the Mineralogical Society of America.
The published version is subject to change. Cite as Authors (Year) Title. American Mineralogist, in press.
DOI: https://doi.org/10.2138/am-2022-8708. http://www.minsocam.org/

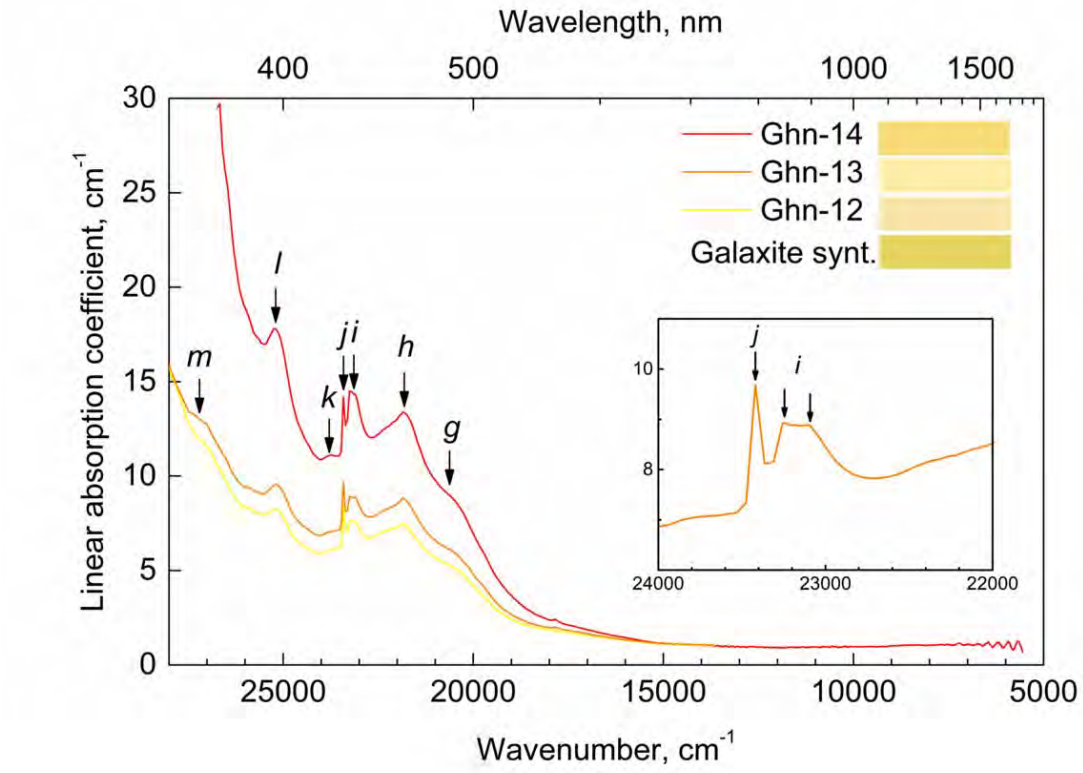

853

854

855

856

857 Fig. 6.

858

859

Always consult and cite the final, published document. See http:/www.minsocam.org or GeoscienceWorld

This is the peer-reviewed, final accepted version for American Mineralogist, published by the Mineralogical Society of America.
The published version is subject to change. Cite as Authors (Year) Title. American Mineralogist, in press.
DOI: https://doi.org/10.2138/am-2022-8708. http://www.minsocam.org/

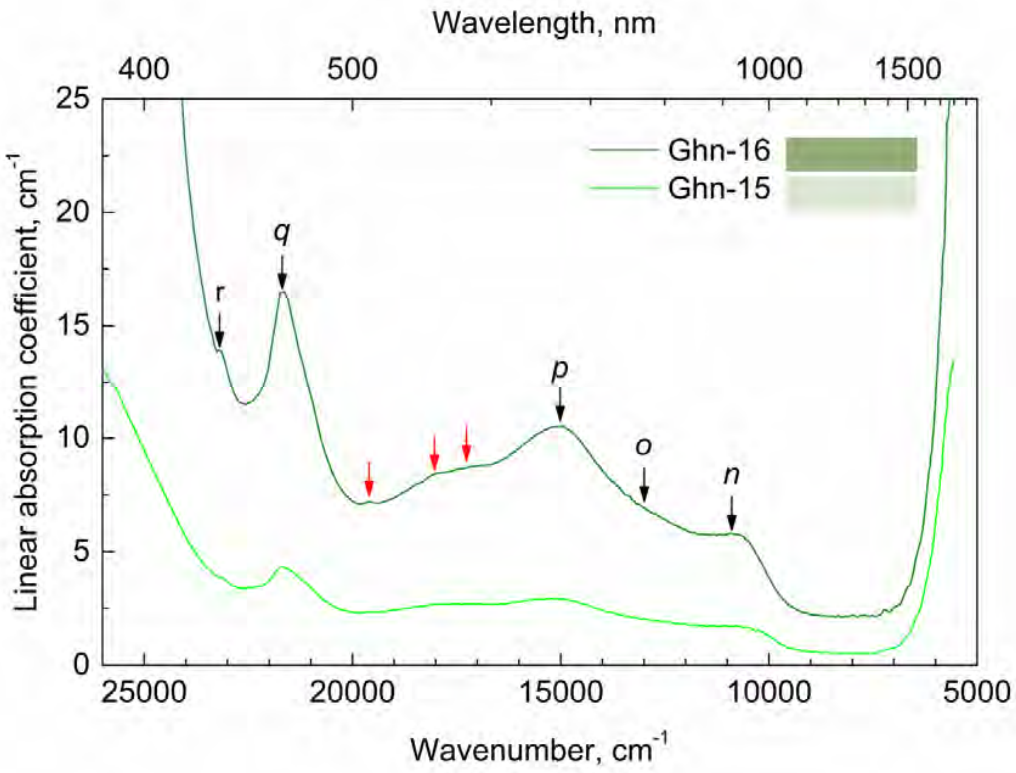

Fig. 7.

Always consult and cite the final, published document. See http:/www.minsocam.org or GeoscienceWorld

This is the peer-reviewed, final accepted version for American Mineralogist, published by the Mineralogical Society of America.
The published version is subject to change. Cite as Authors (Year) Title. American Mineralogist, in press.
DOI: https://doi.org/10.2138/am-2022-8708. http://www.minsocam.org/

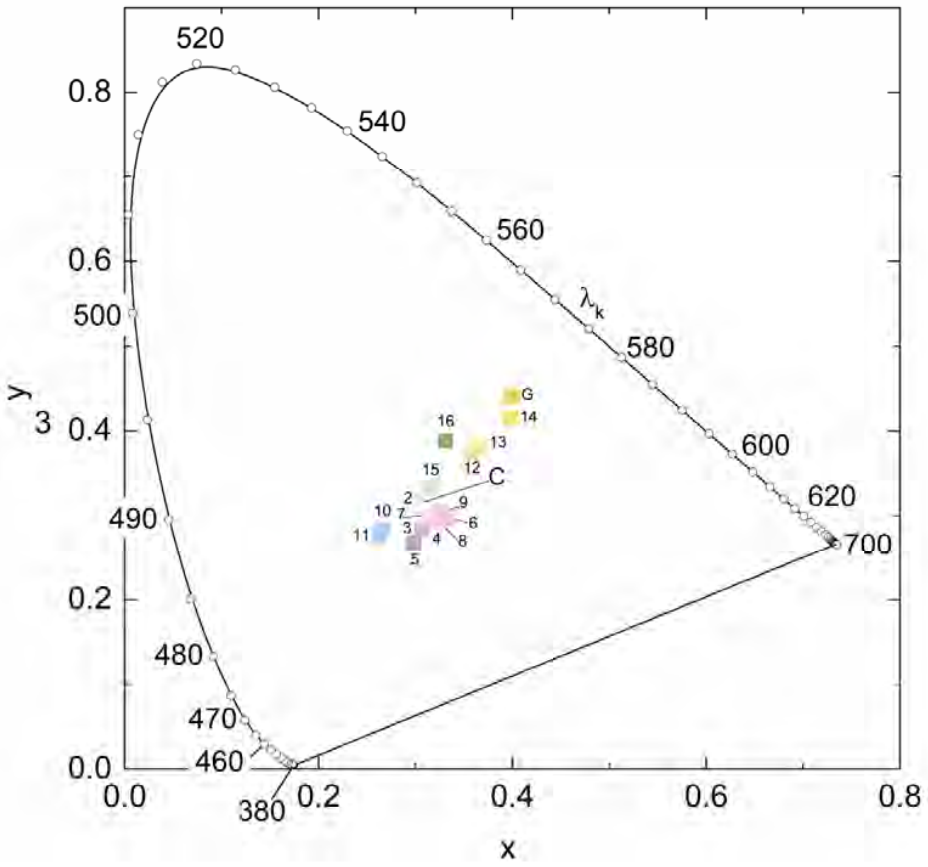

871

872

873

874 Fig. 8.

875

Always consult and cite the final, published document. See http:/www.minsocam.org or GeoscienceWorld

This is the peer-reviewed, final accepted version for American Mineralogist, published by the Mineralogical Society of America.
The published version is subject to change. Cite as Authors (Year) Title. American Mineralogist, in press.
DOI: https://doi.org/10.2138/am-2022-8708. http://www.minsocam.org/

721 Supplementary Table 1. Chromaticity coordinates for the various synthetic gahnites.

722

Sample	Chromaticity coordinates			
	x	y	λ_k	p_c
Ghn-2	0.306	0.318	497	0.013
Ghn-3	0.307	0.283	555'	0.127
Ghn-4	0.321	0.293	519'	0.113
Ghn-5	0.298	0.268	561'	0.173
Ghn-6	0.335	0.298	500'	0.118
Ghn-7	0.316	0.298	528'	0.082
Ghn-8	0.325	0.295	508'	0.115
Ghn-9	0.322	0.302	505'	0.080
Ghn-10	0.266	0.280	480	0.186
Ghn-11	0.262	0.276	480	0.206
Ghn-12	0.358	0.373	575	0.281
Ghn-13	0.367	0.383	575	0.332
Ghn-14	0.398	0.416	576	0.502
Ghn-15	0.317	0.334	566	0.065
Ghn-16	0.331	0.388	563	0.251
Galaxite	0.400	0.440	573	0.574

723

724 ' – supplementary predominant wavelength for purple colors that do not have

725 monochromatic spectral analogous.

726

Always consult and cite the final, published document. See http:/www.minsocam.org or GeoscienceWorld

This is the peer-reviewed, final accepted version for American Mineralogist, published by the Mineralogical Society of America.
The published version is subject to change. Cite as Authors (Year) Title. American Mineralogist, in press.
DOI: https://doi.org/10.2138/am-2022-8708. http://www.minsocam.org/

Supplementary Figures

Supplementary Fig. 1. Photo of 12 gahnite crystals after the first stage of preparation (grinding and polishing on both sides to a thickness of about 1 mm), still glued on the surface of a glass plate with epoxy. At a later time, for spectroscopic measurements the samples were detached from the glass plate and cleaned from epoxy, some crystals were re-polished, decreasing the thickness (see Table 1), which was done to allow improved spectroscopic measurement recordings. Four additional samples (Ghn-3, Gh-9, Gh-12 and Gh-13) were likewise prepared and investigated.

Supplementary Fig. 2. The UV-VIS-NIR regions of the electromagnetic spectrum (https://researchguides.library.wisc.edu/c.php?g=241913&p=1611659).

Supplementary Fig. 3. The CIE 1931 color space chromaticity diagram describing the dominant wavelength, λ_k, for the spectral colors and the supplementary wavelength, λ_k', for purple colorations. The boundary curve is the spectral (or monochromatic) locus with wavelengths shown in nanometers. The straight line gives the loci of the most saturated purple colors consisting of mixtures of red and blue light. Here, there is no appropriate monochromatic λ_k value and, therefore, the value of the supplementary spectral color λ_k' is used.

Supplementary Fig. 4. Tanabe-Sugano diagram for the electronic d^2 configuration. The dashed line represents $^{IV}Ni^{2+}$ in spinel $MgAl_2O_4$ with a crystal field splitting of $\Delta = 5040$ cm^{-1} and the Racah parameter $B = 356$ cm^{-1}. The energy of the $^3T_1$ (^3F) $\rightarrow$ $^3A_1$ (^3F) transition of 9548 cm^{-1} is slightly greater than that of $^3T_1$ (^3F) $\rightarrow$ $^3T_1$ (^3P) of 9300 cm^{-1}. The three levels $^3T_1$, $^3T_2$ and $^3A_2$ are shown by bold lines because they have maximum triplet spin-multiplicity. Electronic transitions between them are spin allowed.

Always consult and cite the final, published document. See http:/www.minsocam.org or GeoscienceWorld

This is the peer-reviewed, final accepted version for American Mineralogist, published by the Mineralogical Society of America.
The published version is subject to change. Cite as Authors (Year) Title. American Mineralogist, in press.
DOI: https://doi.org/10.2138/am-2022-8708. http://www.minsocam.org/

807 Supplementary Fig. 5. Tanabe-Sugano diagram for the electronic d^8 configuration. The dashed line
808 represents $^{VI}Ni^{2+}$ in spinel $MgAl_2O_4$ with a crystal field splitting of $\Delta = 9800$ cm^{-1} and the Racah
809 parameter $B = 907$ cm^{-1}. The calculated energy of the spin-allowed transition $^3A_{2g} \rightarrow {}^3T_{1g}$ (^3P) is
810 27009 cm^{-1}. The three levels $^3A_{2g}$, $^3T_{2g}$ and $^3T_{1g}$ are shown by bold lines because they have
811 maximum triplet spin-multiplicity. Electronic transitions between them are spin allowed.
812
813 Supplementary Fig. 6. Intensity of band *b* as a function of nickel content per-formula-unit for
814 gahnites Ghn-2 to Ghn-9 (Table 1). The line is a linear least-squares best fit to the data.
815
816
817
818
819
820
821

Always consult and cite the final, published document. See http:/www.minsocam.org or GeoscienceWorld

This is the peer-reviewed, final accepted version for American Mineralogist, published by the Mineralogical Society of America.
The published version is subject to change. Cite as Authors (Year) Title. American Mineralogist, in press.
DOI: https://doi.org/10.2138/am-2022-8708. http://www.minsocam.org/

Supplementary Figures

Supplementary Fig. 1.

Always consult and cite the final, published document. See http:/www.minsocam.org or GeoscienceWorld

This is the peer-reviewed, final accepted version for American Mineralogist, published by the Mineralogical Society of America.
The published version is subject to change. Cite as Authors (Year) Title. American Mineralogist, in press.
DOI: https://doi.org/10.2138/am-2022-8708. http://www.minsocam.org/

897

898

899

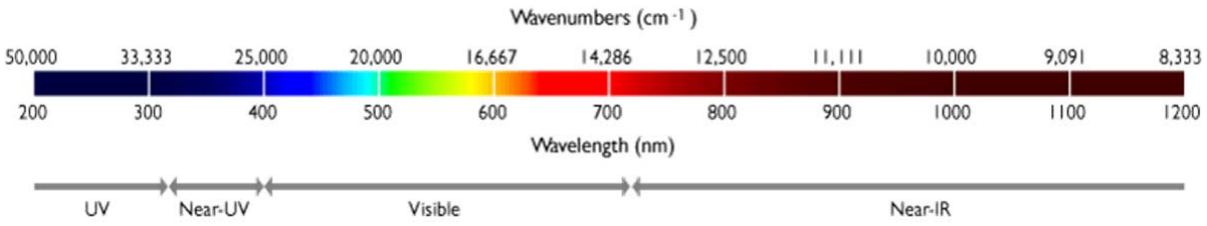

900

901

902

903 Supplementary Fig. 2.

904

Always consult and cite the final, published document. See http:/www.minsocam.org or GeoscienceWorld

This is the peer-reviewed, final accepted version for American Mineralogist, published by the Mineralogical Society of America.
The published version is subject to change. Cite as Authors (Year) Title. American Mineralogist, in press.
DOI: https://doi.org/10.2138/am-2022-8708. http://www.minsocam.org/

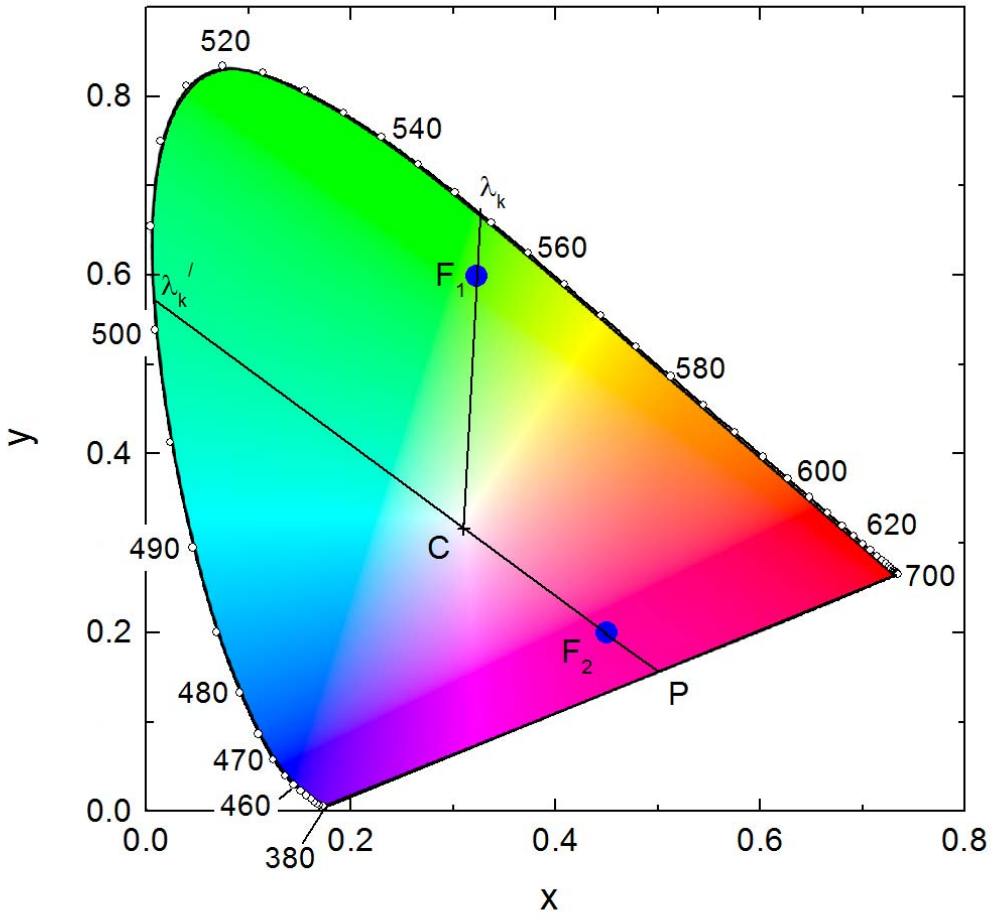

905

906

907

908 Supplementary Fig. 3

909

910

911

912

Always consult and cite the final, published document. See http:/www.minsocam.org or GeoscienceWorld

This is the peer-reviewed, final accepted version for American Mineralogist, published by the Mineralogical Society of America.
The published version is subject to change. Cite as Authors (Year) Title. American Mineralogist, in press.
DOI: https://doi.org/10.2138/am-2022-8708. http://www.minsocam.org/

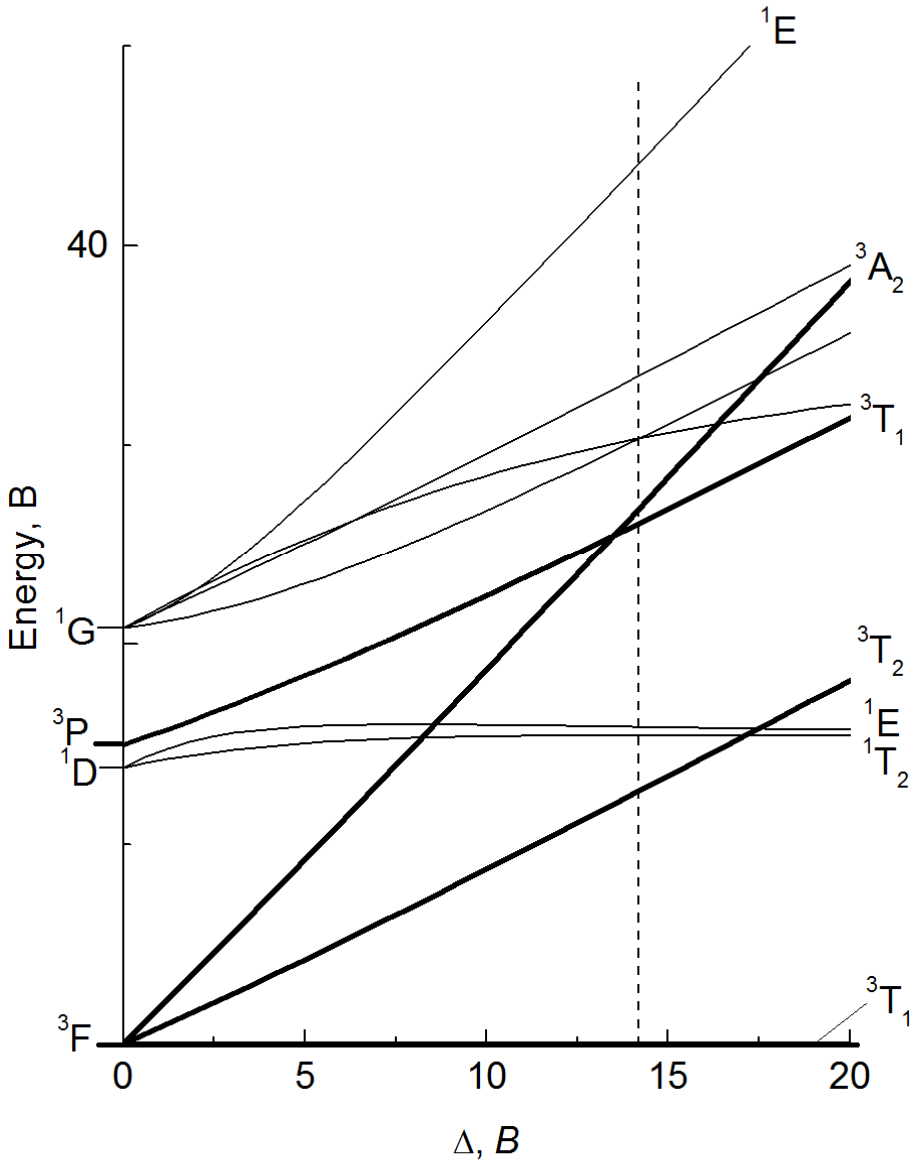

913

914

915 Supplementary Fig. 4.

916

Always consult and cite the final, published document. See http:/www.minsocam.org or GeoscienceWorld

This is the peer-reviewed, final accepted version for American Mineralogist, published by the Mineralogical Society of America.
The published version is subject to change. Cite as Authors (Year) Title. American Mineralogist, in press.
DOI: https://doi.org/10.2138/am-2022-8708. http://www.minsocam.org/

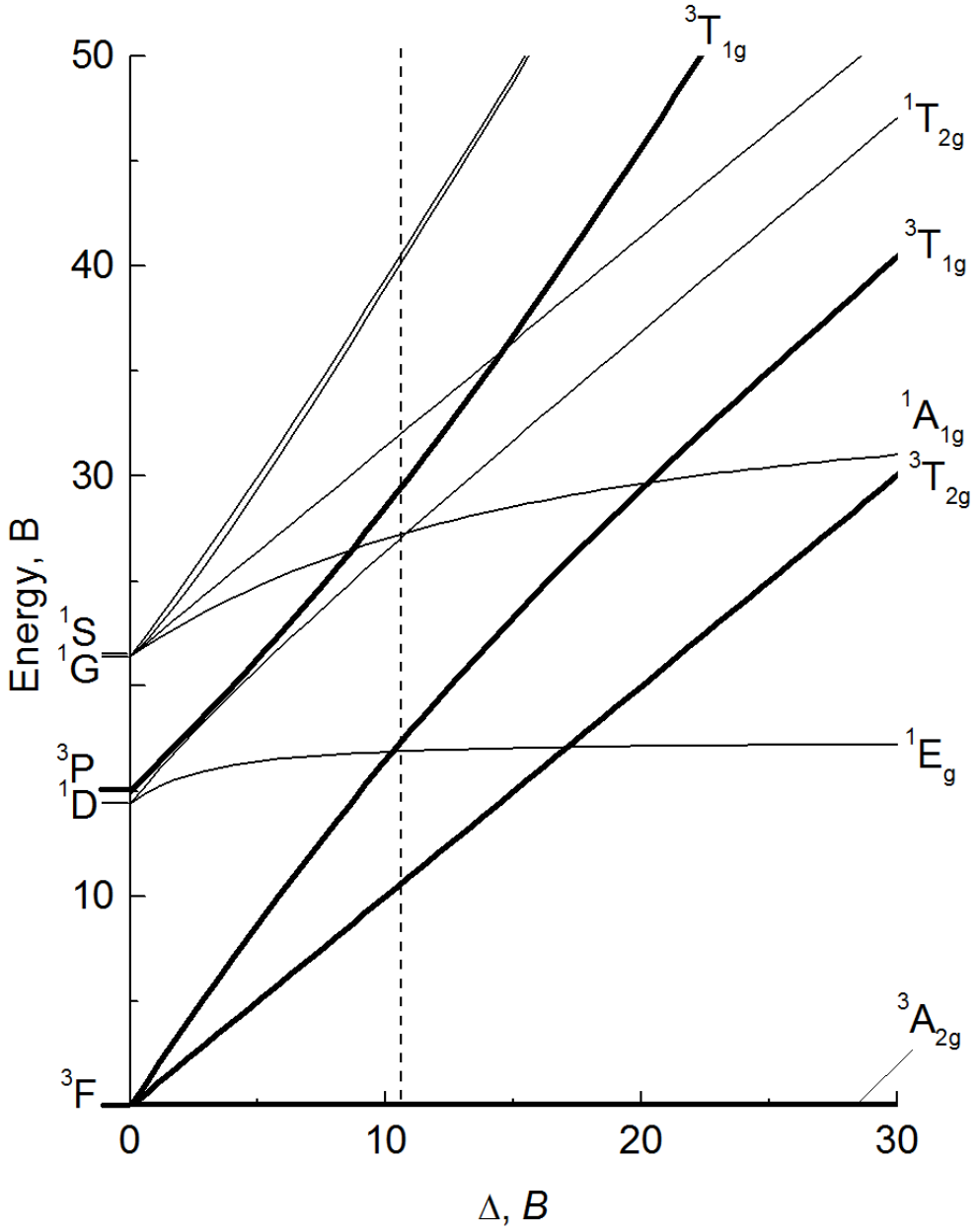

917

918

919 Supplementary Fig. 5.

920

Always consult and cite the final, published document. See http:/www.minsocam.org or GeoscienceWorld

This is the peer-reviewed, final accepted version for American Mineralogist, published by the Mineralogical Society of America.
The published version is subject to change. Cite as Authors (Year) Title. American Mineralogist, in press.
DOI: https://doi.org/10.2138/am-2022-8708. http://www.minsocam.org/

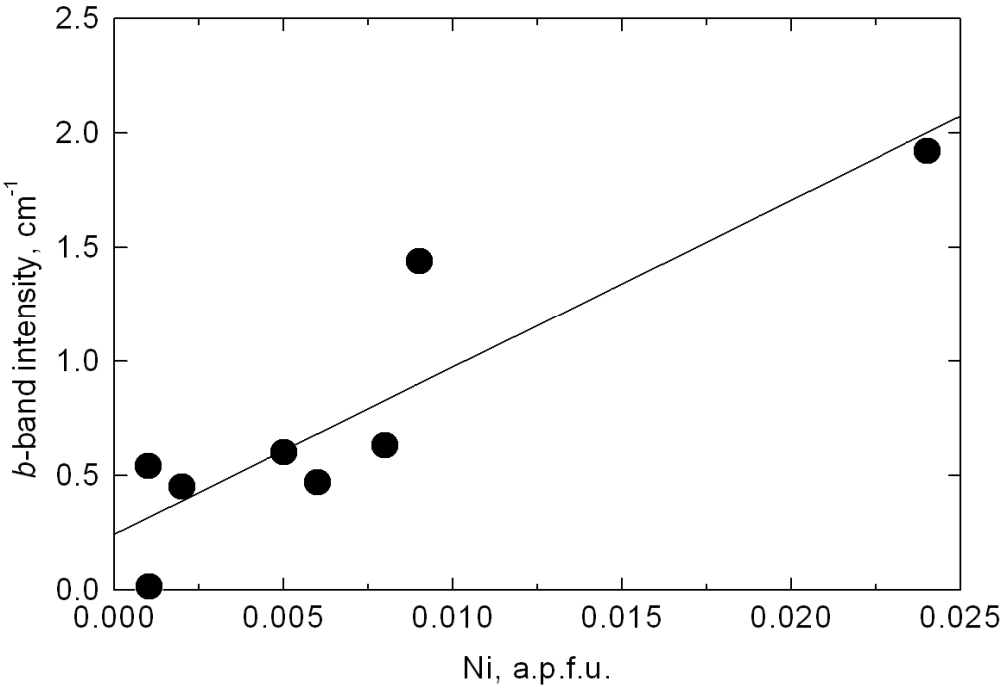

Supplementary Fig. 6.

Always consult and cite the final, published document. See http:/www.minsocam.org or GeoscienceWorld

This is the peer-reviewed, final accepted version for American Mineralogist, published by the Mineralogical Society of America.
The published version is subject to change. Cite as Authors (Year) Title. American Mineralogist, in press.
DOI: https://doi.org/10.2138/am-2022-8708. http://www.minsocam.org/

Supplementary Appendix I

Color is caused by selective absorption of a given illuminating light when it passes through a transparent substance or when it is diffusely reflected from the surface of non-transparent or powder material. Illuminating light often consists of a mixture of different monochromatic radiation occurring in the visible range (Supplementary Fig. 2) in such proportions that the human eye perceives colorless white light. Upon passing through a transparent substance, different wavelength radiation can be selectively absorbed or not and in varous amounts. This selective absorption of radiation in the visible (Vis) region of the electromagnetic spectrum, which is located between the shorter wavelength ultraviolet (UV) and longer wavelength infrared (NIR) regions, results in color.

A colorimetric system be analyzed based on the fact that any color can be reproduced through the mixing of various combinations of other colors[3]. The mixing process can be demonstrated, for example, by projecting various combinations of colored light beams onto the same area of a diffuse reflecting white screen. Here, it can be shown that different combinations of light and their amounts can give rise to the same resultant color. This mixing behavior can also be shown through the blending of various combinations and amounts of colored pigments to produce the same color of paint, for example. The way humans perceive color is a subjective psychological phenomenon, because the precise spectral composition of the mixing colors does not play a role.

The number of combinations of different colors that can mix to produce a certain given color is infinite. This fact is described by Grassman's law, which governs the optical composition of color. It gives the minimal number of colors necessary to reproduce any existing color through mixing and is equal to three and is given by:

$$C_0 = aC_1 + bC_2 + cC_3, \quad (1),$$

[3]We omit any discussion of other types of colorimetric systems, for example, those, based on visual comparison of a sample with color standards (e.g. the Munsel color system – Judd and Wyszecki 1963).

Always consult and cite the final, published document. See http:/www.minsocam.org or GeoscienceWorld

where C_1, C_2 and C_3 are the so-called independent colors. No independent color can be obtained through the mixing of the other two. For instance, they may be red, green and blue. Grassman's law has no physical meaning because it describes the purely psychological aspects of visual color perception. Following (1), any color, C_0, can be expressed three dimensionally and may be represented by the sum of three independent color vectors C_1, C_2 and C_3, whose magnitudes can be different (defined by the coefficients a, b and c). C_1, C_2 and C_3 are called the primary colors or the color stimulus for a given colorimetric system.

The Commission Internationale de l'Eclairage (CIE) in 1931 adopted the first three-stimulus colorimetric system termed *RGB*. The primary colors were red, green and blue having monochromatic wavelengths of 700.0 (*R*), 546.1 (*G*) and 435.8 (*B*) nm, respectively. One has $F = rR + gG + bB$, whereby any color, F, can be made through a mixture of R, G and B taken in the amounts r, g and b. A more convenient representation, where the color stimuli are only additive in nature, and do not necessarily involve subtraction as in the case of some colors of the *RGB* system, is given by the CIE colorimetric system XYZ. Here, the primary colors X, Y and Z are hypothetical and they mix to produce any possible resultant color. This system arises through a mathematical transformation of the *RGB* system. It is based on the same principles, namely, that any color can be specified by the quantities of three different illuminations. The main difference of the XYZ system from the *RGB* system is that the colors of its primary "illuminations" X, Y and Z exist only as colorimetric equations. The colors themselves are not reproduced. The XYZ description forms the basis of all modern colorimetric systems.

The primary colors X, Y and Z are represented by three orthogonal unit vectors and all possible colors, obtained through their mixing, are contained within a closed color-space volume. A color vector, F, can be written as:

$$F = x'X + y'Y + z'X \qquad (2),$$

where x', y' and z' are the coefficients that define the relative amounts of X, Y and Z. Equation (2) describes color quantitatively. For a description of color, the values of chromaticity and brightness

Always consult and cite the final, published document. See http:/www.minsocam.org or GeoscienceWorld

This is the peer-reviewed, final accepted version for American Mineralogist, published by the Mineralogical Society of America.
The published version is subject to change. Cite as Authors (Year) Title. American Mineralogist, in press.
DOI: https://doi.org/10.2138/am-2022-8708. http://www.minsocam.org/

are used. They express the qualitative and quantitative characteristics of color, respectively. Chromaticity is defined by the coordinates:

$$x = \frac{x'}{x' + y' + z'}, y = \frac{y'}{x' + y' + z'} \text{ and } z = \frac{z'}{x' + y' + z'} \quad (3)$$

and, because $x + y + z \equiv 1$, two coordinates suffice for its determination. Usually, x and y are taken. The value of brightness is described by y'. It characterizes the visual perception of light transmittance or reflectance (in the case of non-transparent diffuse reflection) of a substance. The orthogonal chromaticity x-y diagram (Supplementary Fig. 3) is typically used for the illustration of color. It is a two-dimensional projection from the (1,1,1) section in X-Y-Z space, where the orientation of the main color axes is taken in a such way that the X + Y + Z = 1 plane gives a right triangle. Here, all real colors lie in an area bounded by a curve that defines the most saturated spectral colors of monochromatic illuminations in the visible range from 380 to 700 nm and a straight line that connects the ends of this curve. This latter line is the locus of the most saturated purple colors. Point C is the locus of the standard white illuminator, C, representing dispersed North sky daylight.

For a description of chromaticity, the dominant wavelength, λ_k, and the color saturation value, p_c, are typically used. For example, for the color F_1 having the coordinates $x_1 = 0.32$ and $y_1 = 0.6$, λ_k is about 554 nm and $p_c = CF_1/C\lambda_k \cong 0.81$ (Supplementary Fig. 3). λ_k describes the dominant color, which is yellowish-green in this case. p_c gives the amount of spectral color, λ_k (dominant wavelength), which should be mixed with the color white, C, to reproduce the color F_1 having the coordinates x_1 and y_1. In comparison, the color of F_2, which does not have a dominant wavelength, is purple (i.e., a mixture of red and blue light). Its saturation value, p_c, is given, once again, by $p_c = CF_2/CP \cong 0.75$. Instead of using λ_k, the value of the supplementary spectral color $\lambda_k' \sim 502$ nm is taken. All colors, which lay within the triangle defined by 380 nm, point C, and 700 nm (Supplementary Fig. 3), have an infinite number of purple colors that do not have spectral

Always consult and cite the final, published document. See http:/www.minsocam.org or GeoscienceWorld

analogues. Therefore, their λ_k' and p_c values should be determined as done for color F_2. For further aspects behind the colorimetric system XYZ, the reader is referred to Judd and Wyszecki (1975).

Supplementary Appendix II

Hålenius et al. (2007) undertook an analysis of the Racah parameters *B* and *C* and the crystal-field-splitting parameter, $\Delta = 10Dq$, by considering the spectra of a number of Mn^{2+} phases including the spinel galaxite ($Mn^{2+}Al_2O_4$). They labeled the various Mn^{2+} spin-forbidden bands, typically five in number, from ν_1 to ν_5 (see Table 4 in Hålenius et al. 2007) with increasing wavenumber and gave exact equations to calculate the energies of ν_3 and ν_5 and approximate solutions for ν_1, ν_2 and ν_4. In terms of galaxite, *B* and *C* can be calculated from their eqns. (3) and (5) and *Dq* obtained from their eqns. (1) and (2) and in doing this they obtained $B = 627$ cm^{-1}, $C = 3424$ cm^{-1} and $Dq = 592$ cm^{-1}. We note that eqns. (1) and (2) are not real in a strict sense, because if $Dq = 0$, the wavenumber of both ν_1 and ν_2 would be infinite in value, instead of the case where both would have equal energies corresponding to the electronic term ^{4}G (e.g., Burns 1993, Fig. 3.10). Taking the *B*, *C* and *Dq* values for galaxite and inserting them into their eqns. (1) and (2), one calculates $\nu_1 = 19167$ and $\nu_2 = 23389$ cm^{-1}. If, alternatively, one calculates them from the energy matrices of Tanabe and Sugano for the $^4T_1$ and $^4T_2$ states of the electronic configuration d^5 (i.e., Sviridov et al. 1976) and assuming a Trees parameter of $\alpha = 0$, one obtains $\nu_1 = 19745$ and $\nu_2 = 22145$ cm^{-1}. These values agree better with the experimental spectroscopic values for these transitions of 20300 and 22250 cm^{-1}, respectively. Note also that when $Dq = 0$, one has $\nu_1 = \nu_2 = 23390$ cm^{-1} for the electronic term ^{4}G. Similarly, the calculated wavenumber of 26529 cm^{-1} for band ν_4 (i.e, the $^6A_1(S) \rightarrow {}^4T_{2g}(D)$ transition) in galaxite, as obtained from its energy matrix, is closer to the experimental value 25970 cm^{-1} compared to the value of ~25271 cm^{-1} calculated from eqn. (4) of Hålenius et al. (2007). However, in spite of the various differences, if one considers the uncertainties associated with

Always consult and cite the final, published document. See http:/www.minsocam.org or GeoscienceWorld

crystal-field and Racah-parameter theory, we think eqns. (1), (2) and (4) give roughly similar wavenumbers to those calculated using energy matrices.

Assuming that the wavenumbers of the two field-independent electronic transitions $^6A_1 \rightarrow {}^4A_1$, ^4E (^4G) (band ν_3 of Hålenius et al. 2007), as given by the mean wavenumber value for bands i and j, and that the wavenumber value of band m (i.e., ν_5 with $^6A_1(S) \rightarrow {}^4E(D)$) - see Table 2 - we obtain for our Mn gahnites $B = 561$ and $C = 3530$ cm^{-1}. We also calculated the wavenumber for the two field-dependent electronic transitions $^6A_1 \rightarrow {}^4T_1(G)$ and $\rightarrow {}^4T_2(G)$, labled ν_1 and ν_2, respectively (Hålenius et al. 2007), in the gahnites studied here, using their energy matrices (Sviridov et al. 1976). Ideally, the calculated wavenumber values of ν_1, ν_1 and ν_4 should agree with their experimental values for the same value of *Dq* (c.f. Burns 1993 - Fig. 3.16). This is always the case for ν_3 and ν_5, because they are field independent (i.e., a function of *B* and *C* but not of *Dq*) and *B* and *C* are calculated from their energies. However, we obtain an equivocal result for $^4T_1(G)$ and $^4T_2(G)$ that best agree with the experimental values of 20730 and 21910 cm^{-1} for rather different values of *Dq*, that is, 472 and 596 cm^{-1}, respectively. Adopting a mean intermediate value of $Dq = 534$ cm^{-1}, one calculates $\nu_1 = 20213$ and $\nu_2 = 23251$ cm^{-1}. They differ significantly from the experimental values of 20730 and 21910 cm^{-1} (i.e., +517 and -1305 cm^{-1}, respectively).

Concluding, we think that the noted disagreements between experiment and theory in our analysis are mainly due to the fact that the tetrahedrally coordinated Mn^{2+} in our gahnites is distorted from regular tetrahedral symmetry. This proposal is supported by the observed splitting and fine structure of the electronic bands $^6A_1 \rightarrow {}^4T_2$ and $^6A_1 \rightarrow {}^4A_1$, ^4E (^4G) shown in the spectra of Fig. 6 (see also Table 2). Therefore, the energy matrices that assume cubic symmetry (Sviridov et al. 1976) are not applicable. Moreover, we think that the Racah parameters *B* and *C* probably cannot be determined from the wavenumbers of the strongly split $^6A_1 \rightarrow {}^4A_1$, ^4E (^4G), i.e. i and j bands, and band m (Fig. 6) assigned to $^6A_1(S) \rightarrow {}^4E(^4D)$. It is also of note that the ratio $C/B \approx 6.3$ significantly differs from the "typical value" of 3.5 obtained for various Mn^{2+}-bearing phases (e.g., Burns 1993 -

Always consult and cite the final, published document. See http:/www.minsocam.org or GeoscienceWorld

This is the peer-reviewed, final accepted version for American Mineralogist, published by the Mineralogical Society of America.
The published version is subject to change. Cite as Authors (Year) Title. American Mineralogist, in press.
DOI: https://doi.org/10.2138/am-2022-8708. http://www.minsocam.org/

Table 11.1). This indicates that the Racah parameters *B* and *C*, based on our analysis and the use energy equations for ν_3 and ν_5 (Hålenius et al. 2007), can not be determined quantitatively.

Always consult and cite the final, published document. See http:/www.minsocam.org or GeoscienceWorld